Geoscience Frontiers 15 (2024) 101727

Contents lists available at ScienceDirect

Geoscience Frontiers

journal homepage: www.elsevier.com/locate/gsf

Research Paper

Geophysical evidence of a large occurrence of mud volcanoes associated with gas plumbing system in the Ross Sea (Antarctica)

Martina Busetti *, Riccardo Geletti, Dario Civile, Chiara Sauli, Giuseppe Brancatelli, Edy Forlin, Daniela Accettella, Lorenza Barro Savonuzzi, Laura De Santis, Aldo Vesnaver, Andrea Cova

National Institute of Oceanography and Applied Geophysics – OGS, Borgo Grotta Gigante 42/c, 34010 Sgonico, Trieste, Italy

ARTICLE INFO

Article history:
Received 29 June 2023
Revised 11 August 2023
Accepted 6 October 2023

Handling Editor: M. Yoshida

Keywords:
Ross Sea
Antarctica
Mud volcanoes
Gas plumbing system
Gas hydrate
Bottom Simulating Reflector

ABSTRACT

Seafloor and buried reliefs occur along continental margin of the Ross Sea (Antarctica). These features are several kilometres wide and tens of metres high, exhibiting cone or flat-top dome shapes. Previous studies have proposed a volcanic or glacial origin for these formations, but these hypotheses do not account for all the available evidence.

In this study, we use morpho-bathymetric data, intermediate resolution multichannel seismic and high resolution chirp profiles, as well as magnetic lines to investigate these clusters of mounds. By employing targeted processing techniques to enhance the geophysical characterization of the seafloor and buried reliefs, and to understand the underlying geological features, we propose that the reliefs are mud volcanoes. Some of these formations appear to be associated with a plumbing system, as indicated by acoustic anomalies linked to sediment containing gas. These formations are likely fed by clayey source rocks of Miocene age. Additionally, other reliefs might be the result of mud mobilisation caused by gravity instability and fluid overpressure.

1. Introduction

The Ross Sea continental shelf has been extensively studied especially for paleoclimatic and tectonic purposes. Geophysical surveys have been carried out since the 1980s by many countries, and although the focus at the time was on regional studies, some buried and outcropping isolated or fields of reliefs of unclear origin have intrigued researchers ever since.

Cooper et al. (1987) and Brancolini et al. (1995) proposed a volcanic origin for several tens of metres high and up to several kilometres wide conical and flat-topped highs located on the seafloor in the western Ross Sea, south of the Drygalski Ice Tongue. This interpretation is based on the location of these reliefs on the Lee Arch, a N-S trending structural high that connects the huge and active Melbourne and Erebus volcanoes (Fig. 1), and presents magmatic intrusions, submerged volcanoes and volcanic islands (e.g., the Franklin Islands). A magmatic origin for the same flat-topped reliefs was also suggested by Lawver et al., (2007, 2012) based on a multidisciplinary geophysical dataset including swath bathymetry, magnetic and gravimetric models. The authors interpreted these reliefs as tuyas, a type of flat-topped and steep-sided subglacial volcano.

A magmatic origin was also suggested for buried morphological reliefs in the northwestern Ross Sea on the basis of targeted reprocessing of multichannel seismic data, seismic tomography, magnetic and gravity analyses (Boehm et al., 1993; Geletti et al., 1993). These investigations revealed high velocities and magnetic contrasts between the buried reliefs and the surrounding sediments, so they were interpreted as magmatic intrusions, although this hypothesis was not univocal and not entirely satisfactory with the observation of the data (Boehm et al., 1993).

A new perspective on the origin of the seafloor morphologies in the western Ross Sea, was proposed by Geletti and Busetti (2011). These authors interpreted two reliefs, named Tergeste and Iulia, as mud volcanoes associated with the presence of gas chimneys. This hypothesis was based on the discovery of a Bottom Simulating Reflector (BSR) on the seismic profiles beneath the two cone-shaped reliefs. The BSR is the geophysical evidence of the interface between the gas hydrate-bearing sediments and the free gas-bearing sediments, highlighted by an abrupt negative change in acoustic impedance. Mud volcanoes are the result of the extrusion of mud, rock fragments and fluids caused by the release of mud trapped at depth and overpressure fluids that rise to the seafloor

* Corresponding author.
E-mail address: mbusetti@ogs.it (M. Busetti).

https://doi.org/10.1016/j.gsf.2023.101727

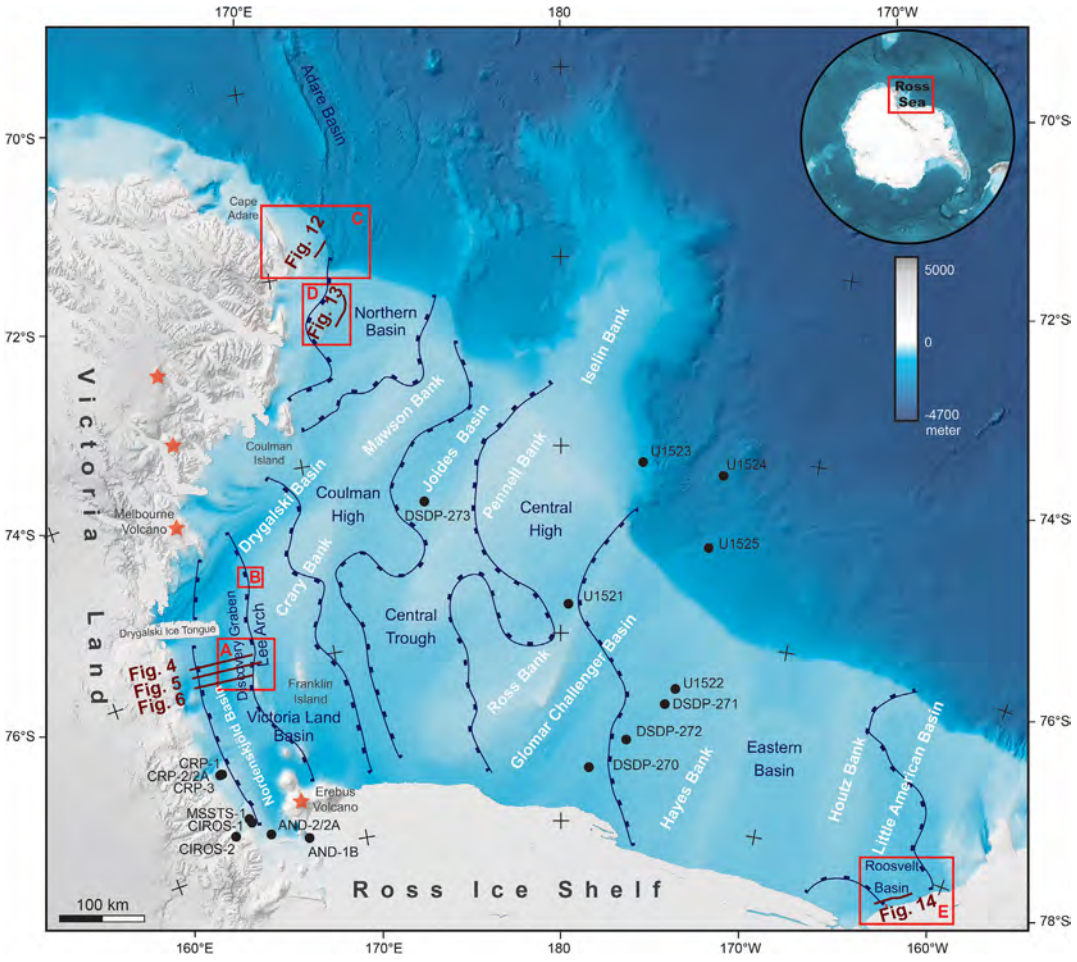

Fig. 1. The IBCSO morpho-bathymetry and topography of the Ross Sea (Dorschel et al., 2022) with the location of the study areas (red rectangles) and seismic lines (in brown). The outlines of the tectonic basins and highs and their names are indicated in dark blue. The names of the morphological basins and highs are indicated in white. Black dots indicate the locations of the boreholes and the red stars indicate the active volcanoes.

along fractures and faults. The fluids enter in the water column while the sediment deposition produces the mud volcanoes (Mazzini and Etiope, 2017).

Buried reliefs were described in the Roosevelt sub-basin, a sedimentary depocenter of the Eastern Basin located in the southeasternmost part of the Ross Sea (Fig. 1). They appear as flat-topped ridges separated by narrow troughs and buried below ca. 200 m of sediment. These reliefs were interpreted as a submerged glacial moraine (Sorlien et al., 2007), although a mud volcano origin was more recently suggested by Barro Savonuzzi et al. (2023).

The aim of this work, based on the interpretation of various geophysical data, such as reprocessed multichannel seismic profiles, magnetic profiles, high resolution chirp profiles, and morpho-bathymetric data, is to improve the understanding of the origin of the widespread enigmatic seafloor and buried morphological reliefs occurring in different areas of the whole Ross Sea (Fig. 1), linking their origin to the presence and migration of free gas along pipes, chimneys, and fault conduits.

2. Geological setting

The Ross Sea is a large embayment of the Antarctic continental margin, about 1000 km × 750 km wide, southward delimited by the Ross Ice Shelf. A Late Cretaceous and Cenozoic sedimentary sequence is distributed in four major rifting depocenters: Victoria Land Basin (VLB), Northern Basin (NB), Central Trough (CT), and Eastern Basin (EB), (Brancolini et al., 1995) (Fig. 1).

The Victoria Land Basin is the westernmost and deepest basin of the Ross Sea containing several kilometres of sediments, and affected by oblique rifting and transtensional faulting since the late Oligocene (Cooper et al., 1987; Brancolini et al., 1995; Salvini et al., 1997). The Terror Rift (TR) developed within the VLB during the last and most recent Neogene rifting phase and consists of the down-faulted Discovery Graben and the adjacent magmatically intruded and tectonically active Lee Arch (Cooper et al., 1987; Sauli et al., 2021) which connects the two active volcanoes Erebus and Melbourne and is part of the McMurdo Volcanic Group (Kyle et al., 1992). Some seamounts north of Ross Island were directly dredged (Rilling et al., 2009) supporting the presence of the Cenozoic submarine and subaerial volcanism of the McMurdo Volcanic Group (Kyle et al., 1992).

The Northern Basin lies on the northwestern continental shelf and accommodates up to 6 km of Oligocene-Miocene sediments (Brancolini et al., 1995) overlain by Late Pliocene and Quaternary prograding glacio-marine sediments deposited and shaped by the glacial and interglacial oscillations of the ice sheets, and also by the North Victoria Land marine-terminating glaciers onto the mid-outer shelf (Bart et al., 2000, 2011; Sauli et al., 2014; Pérez et al., 2022). The magmatic rocks of the Cape Hallett Province (Smellie et al., 2011), crop out along the margin of North Victoria Land.

The Central Trough consists of two depocenters, with the northern one offset to NE respect the southern one, and filled with about 4–6 km of Cenozoic glacio-marine sediments (Brancolini et al., 1995; Chow and Bart, 2003), as well as the largest Eastern Basin (EB) to the east (Brancolini et al., 1995). The latter includes the ~3 km deep Roosevelt sub-basin, in the south-easternmost part (Sorlien et al., 2007).

The stratigraphy of the Ross Sea basins, which has been extensively studied by calibrating the seismic dataset with borehole data (Fig. 2), is characterised, from bottom to top by Paleogene continental to marine deposits and proglacial/subglacial sediments deposited at least since the Oligocene/Early Miocene, indicating an increase of the glacial influence associated with the climate cooling, i.e. the ice growth, advance and grounding on the mid-outer continental shelf. The Antarctic Offshore Stratigraphy (ANTOSTRAT) Atlas provides for the Ross Sea the recognition of 8 seismic units (RSS) bounded by six major (shelf-wide) erosional unconformities (RSU) from 1 to 6, (Brancolini et al., 1995) calibrated by the Deep Sea Drilling Project (DSDP) sites (Hayes et al., 1975; Savage and Ciesielsky, 1983). This subdivision is still in use but it has evolved by new dating, revision of age-depth models and the improvement of the seismic correlations through the entire available boreholes and throughout the all basins. The updates were allowed by the new acquired seismic data (see Antarctic Seismic Data Library System; https://sdls.ogs.trieste.it), the Cape Roberts Project (CRP) drilling on the western margin of the VLB (Cape Roberts Science Team, 1998, 1999, 2000; Davey et al., 2000; Hamilton et al., 2001), the Antarctic Geological Drilling Project (ANDRILL) carried out in the southern part of the VLB on the east and west sides of Ross Island (Horgan et al., 2005; Naish et al., 2007, 2009; Fielding et al., 2008; Pekar et al., 2013), and the most recent International Ocean Discovery Program (IODP) with the Expedition 374 in the eastern outer shelf and rise of the Ross Sea (McKay et al., 2019; Pérez et al., 2021, 2022).

Glacial processes have deeply shaped the physiography of the Ross Sea: the loading of the ice caps on the continent and the

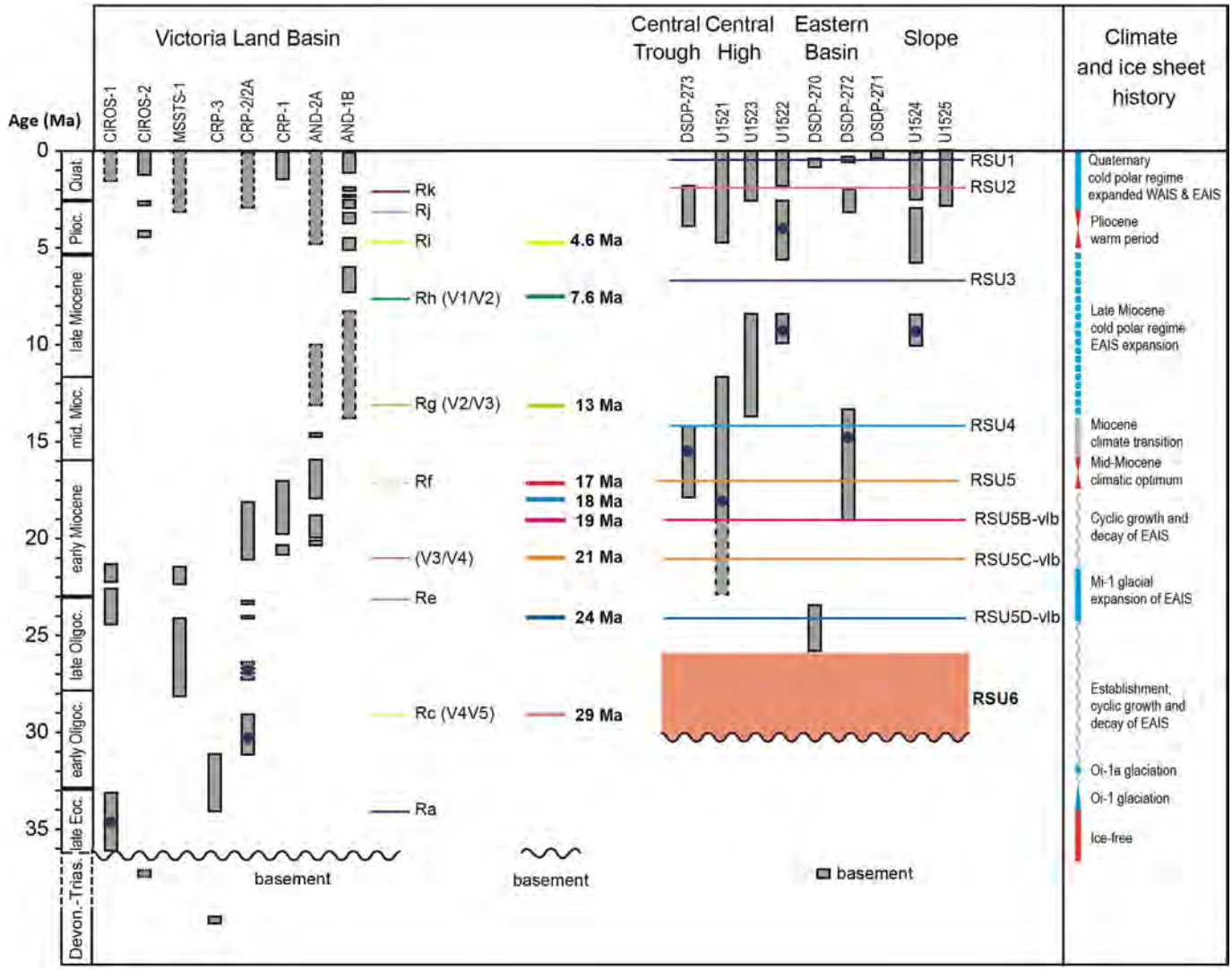

Fig. 2. Time-distribution of the well stratigraphy (see Fig. 1 for position) and regional seismic reflectors/unconformities for the Ross Sea (modified after Fielding, 2018; Sauli et al., 2021) with hydrocarbon occurrences (blue dots). Climate and ice sheet history from Fielding (2018). Stratigraphy of the wells CIROS-1 (Barrett, 1986, 1989), CIROS-2 (Barrett and Staff, 1985), CRP-1, CRP2/2A and CRP-3 (Cape Roberts Science Team, 1998, 1999, 2000), AND-1B and AND2/2A (SMS Science Team, 2010), DSDP-270, -271, -272, -273 (Hayes et al., 1975; Savage and Ciesielsky, 1983; Kulhanek et al., 2019), and IODP U1521, U1522, U1523 (Mackay et al., 2019) are correlated with the main seismic reflectors and unconformities. Victoria Land Basin: Ra to Rk unconformities from Fielding et al. (2008) and V1 to V5 from Cooper et al. (1987), reflectors from 4.6 Ma to 29 Ma from Sauli et al. (2021); reflectors 17, 21 and 29 Ma from Hamilton et al. (2001) and Fielding (2018). Ross Sea: ANTOSTRAT Ross Sea Unconformities RSU1 to RSU6 from Brancolini et al. (1995), with further integration of RSU5B_vlb, RSU5C_vlb and RSU5D_vlb from Sauli et al. (2021).

glacial erosion overdeepened and foredeepened the continental shelf (ten Brink, U.S. et al., 1995). Erosion by ice streams through time resulted in the formation of valleys and banks that do not always overlap with tectonic basins and structural highs. Exceptions are the Nordenskjöld and Drygalski basins, which coincide with the tectonic Discovery Graben and the Northern Basin (Fig. 1). The present-day seafloor of the Ross Sea preserves erosional and depositional features reflecting the modes of advance and retreat of grounded ice sheets and ice streams during and after the Last Glacial Maximum (LGM; e.g., Ship et al., 1999; Prothro et al., 2020 and ref. therein).

2.1. Free gas and gas hydrates in the Ross Sea

The presence of gas in Ross Sea sediments was detected at several drill sites (Fig. 2). Low gas concentrations (mainly methane and to a lesser extent ethane) were found in shallow sediments sampled by gravity cores (Rapp et al., 1987), DSDP (McIver, 1975) and IODP drilling (McKay et al., 2019). At the DSPD-272 (Eastern Basin) and DSDP-273 (Central Trough) sites, a slight increase of gas was found in Late to Middle Miocene mudstone and diatom-bearing mudstone sediments, with maximum values of 179,000 ppmv and 147,000 ppmv of total hydrocarbon gas (mainly methane) content, respectively (McIver, 1975). The gas isotopic analyses revealed very negative $\delta^{13}C$ values indicating a probable shallow biogenic origin (Claypool and Kvenvolden, 1983).

In the IODP sites drilled in the eastern Ross Sea, the gas content is generally low and below the detection limit in the upper part of all sites, from 50 m to 140 m of Pleistocene sediment. The relatively highest contents were found in Early Miocene to Pliocene mudstone, diatom-bearing/rich mudstone and diamicton: (i) in the U1521 site the gas concentrations are low and increase downhole reaching the maximum values of 67,000 ppmv methane and 264 ppmv ethane in Early Miocene sediment, with a mixed input of terrestrial and marine-derived organic matter; (ii) in the U1522 site maximum value of 65,000 ppmv of methane was found in the Pliocene sediment and a lower concentration in the Late Miocene sediment, and is likely formed by methanogenic bacteria; (iii) in the U1524 site almost 60,000 ppmv of methane and 120 ppmv of ethane were found in the Late Miocene - Pliocene sediment, with the highest concentration in the diatom rich mudstone (McKay et al., 2019).

In the western Ross Sea, in the CIROS-1 well, the total organic carbon values (TOC) are all low, ranging from 0.21 % to 0.66 %, with an average of 0.34 %, and increase slightly down in Oligocene to Early Miocene rocks (Collen et al., 1989), whereas 0.66 % of TOC, likely residue from migrated hydrocarbons, was identified in a 2 m thick late Eocene sandstone, derived from terrestrial and marine organic material (Cook and Woolhouse, 1989).

At the Cape Roberts CRP-2/2A site, although the measured gas content is low, values of 0.66–0.70 % TOC were found in correspondence of two levels of diatom rich mudstone of Early and Late Oligocene age respectively (Cape Roberts Science Team, 1999).

Geophysical evidence for the presence of gas hydrates and free gases feeding mud volcanoes, has been found in the western Ross Sea (Geletti and Busetti, 2011, 2022). Gas hydrates are frozen gas composed mainly of methane and water that form at low temperature and high pressure. The presence of gas hydrate is inferred by identifying a Bottom Simulating Reflector (BSR), a high amplitude reflector that mimics the topography of the seafloor in marine seismic reflection data. The BSR often crosscuts the local stratigraphy as it follows the gas hydrate stability field that is controlled by hydro-lithostatic pressure, seawater temperature and geothermal gradient. Above the BSR, the hydrate gas is present, while below, due to the increase of temperature from the geothermal gradient, the gas is free, and can seep along fractures and faults up to the seafloor, creating pockmarks and mud volcanoes. This dynamic is observed in the Victoria Land Basin where the free gas is present below the BSR and rises along fractures and faults, whereas in the Lee Arch, the free gas appears to be more pervasive.

According to the equilibrium diagram for hydrates of different composition, a predominant methane composition of the gas is plausible (Geletti and Busetti, 2011).

The theoretical occurrence of the Gas Hydrate Stability Zone (GHSZ) was modelled locally in the central Victoria Land Basin by Geletti and Busetti (2011) and regionally for the Ross Sea by Giustiniani et al. (2018). These authors provided evidence for the possible occurrence of gas hydrate at the continental margin of the Ross Sea.

3. Material and methods

This work is based on a geophysical dataset that includes: multichannel seismic profiles (MCS), morpho-bathymetry with multibeam echosounder (MBES), sub-bottom profiles (SBP), magnetic lines. These data were collected by OGS using the R/V OGS Explora in the framework of the Italian National Antarctic Program (PNRA), by the Bundesanstalt für Geowissenschaften und Rohstoffe (BGR; Germany) and by the United States Geological Survey (USGS).

MCS lines used in this paper are available from the Antarctic Seismic Data Library System for Cooperative Research (SDLS; https://sdls.ogs.trieste.it):

- MCS collected in 1988 (line IT88-06) and 1990 (lines IT90AR-63, -64, -65) by the R/V OGS Explora as part of the PNRA and reprocessed by Geletti and Busetti (2011, 2022) and for this paper;
- MCS collected in 1980 (line BGR80-100) by the BGR using the R/V OGS Explora and reprocessed by Barro Savonuzzi et al. (2023);
- MCS data collected as part of the USGS Antarctic Programme (line USGS-414) in 1987 with the R/V S.P. Lee (Cooper et al., 1987) and with the R/V Nathaniel B. Palmer in 2003 as part of cruises NBP0301 (Sorlien et al., 2010). The profile NBP0301-27B used in this paper was reprocessed by Barro Savonuzzi et al. (2023). Most stack profiles are available through the Antarctic SDLS, and field data are available through the Marine Geoscience Data System (https://www.marine-geo.org).

The MBES dataset used in this work is as follows:

- multibeam echo sounder bathymetry data collected in 2006 by OGS as part of the PNRA using the Reson 8111 hull-mounted multibeam echo sounder and processed using Teledyne Reson PDS2000 and Teledyne CARIS softwares;

- multibeam echo sounder bathymetry from 2004 (NBP0401 cruises of USGS) available through the Marine Geoscience Data System (https://www.marine-geo.org) (Lawver and Davis, 2007, 2012);
- SBP profiles collected by OGS in 2006 as part of PNRA through a hull-mounted Benthos CHIRP II with 16 transducers operating at 2–7 kHz;

The magnetic profiles analysed within this work were acquired by OGS along the MCS lines of the PNRA survey as described in Gantar and Zanolla (1993).

The buried and seafloor morphologies were already highlighted in the first elaborations of Boehm et al. (1993) and Geletti et al. (1993), carried out with vintage algorithms, but resumed and refined in this work with the new processing and analysis tools currently available through the industrial software packages Echos® and GeoDepth® from Aspen Technology Inc® at the SEISLAB

laboratory of OGS. The main aims of the MCS reprocessing related to buried and seafloor morphologies were the following: (i) characterization of the velocity field; (ii) analysis of seismic attributes; (iii) enhancement of seismic images; iv) depth migration.

The main acquisition parameters of the analysed seismic profiles are summarised in Table 1. In particular, the acquisition geometry of the OGS MCS profiles was developed for crustal exploration (PNRA OGS Cruise 1987/88) and seismic stratigraphic resolution (PNRA OGS Cruise 1989/90). These parameters, such as cable length, shot interval, and frequency content, in conjunction with the type of source, can provide adequate information on the velocity field characterising the buried bodies and therefore a good quality of the seismic image provided by the profiles migrated to depth.

To highlight the presence of free gas, the amplitude-versus-offset procedures (AVO) and some seismic attributes analysis were applied to selected lines in addition to the profiles in Geletti and Busetti (2011, 2022). In one profile located in the eastern sector of the Discovery Graben, reflection strength and instantaneous frequency (Taner et al., 1979), were computed (Fig. 10b, c). The reflection strength attribute is phase independent and consists of positive values only. High values of the attribute can be used as an effective discriminator because they represent important acoustic impedance contrasts and thus reflectivities correlated with anomalous amplitudes could be associated with gas/fluid accumulations (Taner et al., 1979). The instantaneous frequency attribute is a valuable tool in seismic data analysis, and the analysis of low-frequency anomalies, such as the low-frequency shadow zone (Geletti and Busetti, 2011), can provide clues of potential hydrocarbon indicators, including free gas anomalies. However, comprehensive interpretation and integration with additional data are necessary to make robust assessments and predictions in hydrocarbon exploration.

The applied processing flow allowed us to improve the signal-to-noise ratio, attenuate random noise and multiple reflections, improve the temporal and spatial resolution, and define an accurate velocity field. The flowchart of the processing of MCS profiles NBP-0301-27B in the Roosevelt sub-basin and BGR-80–100 near Cape Adare is described in Barro Savonuzzi et al. (2023). In general, the procedure already tested by Brancatelli et al. (2022) to recover vintage seismic data was applied to all examined profiles. Prestack depth migration (PSDM) was performed for the parts of the seismic sections where the buried bodies occur.

To highlight a few seafloor features in the western Ross Sea using high resolution seismic data (chirp profiles), we processed these data by a simple amplitude-preserving compensation of the geometrical spreading, i.e., just multiplying each time sample by its traveltime (Claerbout, 1985; Denich et al., 2021). In this way, the same scaling function applies to all traces, and the lateral variations of amplitudes depend only on the propagation effects of seismic waves. These effects include both the reflectivity of the seafloor and underlying sediments and diffraction effects. To attenuate the latter ones, we applied a zero-offset time migration based on the phase-shift method (Gazdag, 1978).

4. Results

In the Ross Sea, geophysical data show the presence of kilometre-wide cone-shape and flat-topped reliefs, similar in size and morphology, lying on the seafloor or covered by Late Cenozoic sediments. Seafloor reliefs were identified in three areas in the western Ross Sea, while buried mounds are located in two areas, one in the western and the other in the eastern Ross Sea, where they are underlain by several km thick sedimentary sequences (see Fig. 1 for the location of the study areas). At all sites, there is evidence of gas/fluid occurrence and migration, and the seismic geometries and amplitude anomalies are identified according to the nomenclature described in Løseth et al. (2009) and Andresen (2012).

4.1. The seafloor reliefs in the western Ross Sea

The three areas identified in the western Ross Sea consist of (Fig. 1): a field of several dozen of seafloor reliefs, referred to as OGS Explora Mounds, occurs south of the Drygalski Ice Tongue (area A); a single seafloor relief occurs to the north of the Drygalski Ice Tongue (area B); several seafloor reliefs are located on the northernmost continental margin offshore Adare Peninsula (area C).

The area A has a width of 30 km × 40 km and water depths ranging between 400 m and 650 m b.s.l. where the Lee Arch dips into the more than 1000 m deep Discovery Graben (Fig. 3). The

Table 1
Main acquisition parameters of the multichannel seismic profiles.

	BGR	USGS	OGS	OGS	NBP0301
Line name	BGR80-100	USGS84-414	IT88A-06	IT90AR-63 IT90AR-64 IT90AR-65	NPB0301-27B
Vessel	Explora	S.P. Lee	OGS Explora	OGS Explora	N.B. Palmer
Recording date	1980	1984	1988	1990	2003
Recorder	Texas Instrument DFS V/TI	GUS-HDDR 4200	Sercel SN 358 DMX	Sercel SN 358 DMX	OYO DAS-1
Data length (s)	10	12	12	6	5
Sample rate (ms)	4	2	2	2	1
Field filters	Low 8 Hz 18 dB/oct High 64 hz 72 dB/oct	10–110 Hz	Low 8 Hz, 18 dB/oct High 154 Hz, 18 dB/oct	Low 8 Hz, 18 dB/oct High 154 Hz, 70 dB/oct	
Coverage	24	24	24	60	23
Energy source	Tuned “U” air-gun array 23.45 l 1431 cu.in.	Bolt air-gun array 21.5 l 1311 cu in	2x16 air-gun array 45,16 l 2756 cu. in.	1x16 air-gun array 22,5 l 1373 cu. in.	Sercel GI 105/105 18.44 l 1125 cu.in.
Depth of source (m)	8	10.5	4	4	3
Streamer length (m)	2400	2400	2400	3000	1125
Number of traces	48	24	96	120	45
Groups interval (m)	50	100	25	25	25
Shot interval (m)	50	50	50	25	25
Depth of streamer (m)	12	12–20	5	5	7.5
Near offset (m)	250	297	170	150	25
Far offset (m)	2600	2611	2570	3100	1150

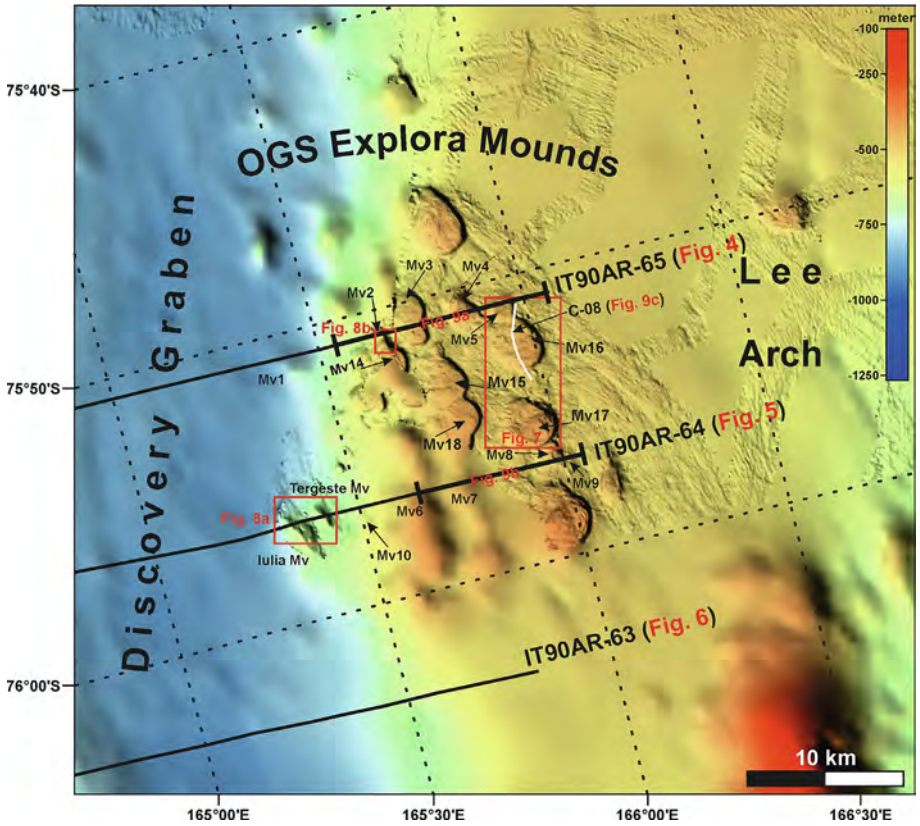

Fig. 3. Morpho-bathymetric map of study area A (see Fig. 1 for location), named OGS Explora Mounds in 2007 (SCAR Composite Gazetteer of Antarctica https://data.aad.gov.au/aadc/gaz/scar), showing the morphologies and distribution of mud volcanoes (Mv) on the structural high of Lee Arch described in the text. The morpho-bathymetric map was produced by merging the low resolution data from the IBCSO (Dorschel et al., 2022) with the high resolution data acquired by OGS in 2006 and USGS data ((http://www.marine-geo.org; Lawver et al., 2007, 2012). The black and white lines indicate the multichannel seismic and chirp profiles used in this study, respectively.

area was named OGS Explora Mounds after the research vessel OGS Explora (SCAR Composite Gazetteer of Antarctica https://data.aad.gov.au/aadc/gaz/scar), which collected the data used in this study in 1990 and 2006. Unfortunately, during the 2006 campaign, the acquisition of morpho-bathymetric data was limited by the presence of sea ice, which prevented optimal coverage of the entire study area and provided information only on some of the mounds identified on the seismic profiles.

The OGS Explora Mounds show two main morphologies: flat-top mounds and cone-shaped reliefs (Figs. 3–10).

The flat-topped mounds occur on the Lee Arch, where the seafloor is a clear erosive surface exposing sediments from the Late Miocene to Plio-Quaternary (Sauli et al., 2021). The mounds show a variable size, with width varying from 700 m to 4000 m and height about 100 m. They may be so close to each other that some of them merge together, along an approximate N–S direction (Fig. 3).

The seismic facies associated with the flat-topped mounds (Mv2, Mv3, Mv4, Mv5 in Figs. 4 and 9, Mv6 and Mv7 in Figs. 5 and 9) consists of subparallel horizons interrupted by fault strands that towards the top assume a more complex geometry, seeped from pipes. Locally, for example below the mounds Mv2 and Mv3 (Fig. 4) a chaotic seismic facies is observed, with faint and discontinuous oblique reflectors downlapping on a high amplitude Downdipping Reflector (DR). The DR deepens towards the west, forming a depression at 200–250 ms buried below sea floor, some tens of milliseconds deep and about 500–1000 m wide (Figs. 4c and 9).

Detailed velocity analysis shows that below the flat-topped mounds there is an average interval velocity of nearly 2000 m/s, with more than one velocity reversal in the underlying sediments (Vp1 in Figs. 4c and 5b). Inside the Mv2, the first velocity inversion occurs at about 50 m b.s.f. from 1800 m/s to 1650 m/s, and the second corresponds to the Downdipping Reflector (DR) at the base of the Mv2 and Mv3, that represents an abrupt change of the interval velocities from 2250 m/s above to 1870 m/s below (Vp1 in Fig. 4c). Outside the mounds, the seismic sequence shows an increase of velocity with depth (Vp2 in Figs. 4c and 5b).

Below the mounds, the seismic facies is characterized by amplitude anomalies such as pipes with blanking vertical anomalies crossing the stratified seismic sequence over several hundred of ms. In some cases, the upper part of the seismic section shows deformation in the form of blowout pipes and extrusions (Figs. 4 and 5).

The seismic section in the Discovery Graben contains several types of seismic anomalies (see the blow-ups of Figs. 4, 5, and 6): (i) discontinuous BSR; (ii) phase reversal and lateral variation of amplitude and frequency along horizons; (iii) low frequency zones and brightening consisting of continuous high amplitude horizons; (iv) wipe-out zones consisting of discontinuous horizons in a mainly faint seismic facies; (v) fault conduits characterized by blanking along the plane usually associated with high amplitude anomalies; (vi) chimneys consisting of about 1 km large and several hundred ms deep vertical features characterized by discontinuous and chaotic bright horizons inside; (vii) several hundred metres to 3 km wide forced-folding with low amplitude and chaotic reflectors laterally surrounded by stratified, not folded reflectors (Figs. 4, 5 and 6).

The seismic profiles show several pockmarks (Figs. 4, 6 and 8) and a diatreme, a volcanic chimney associated with gaseous

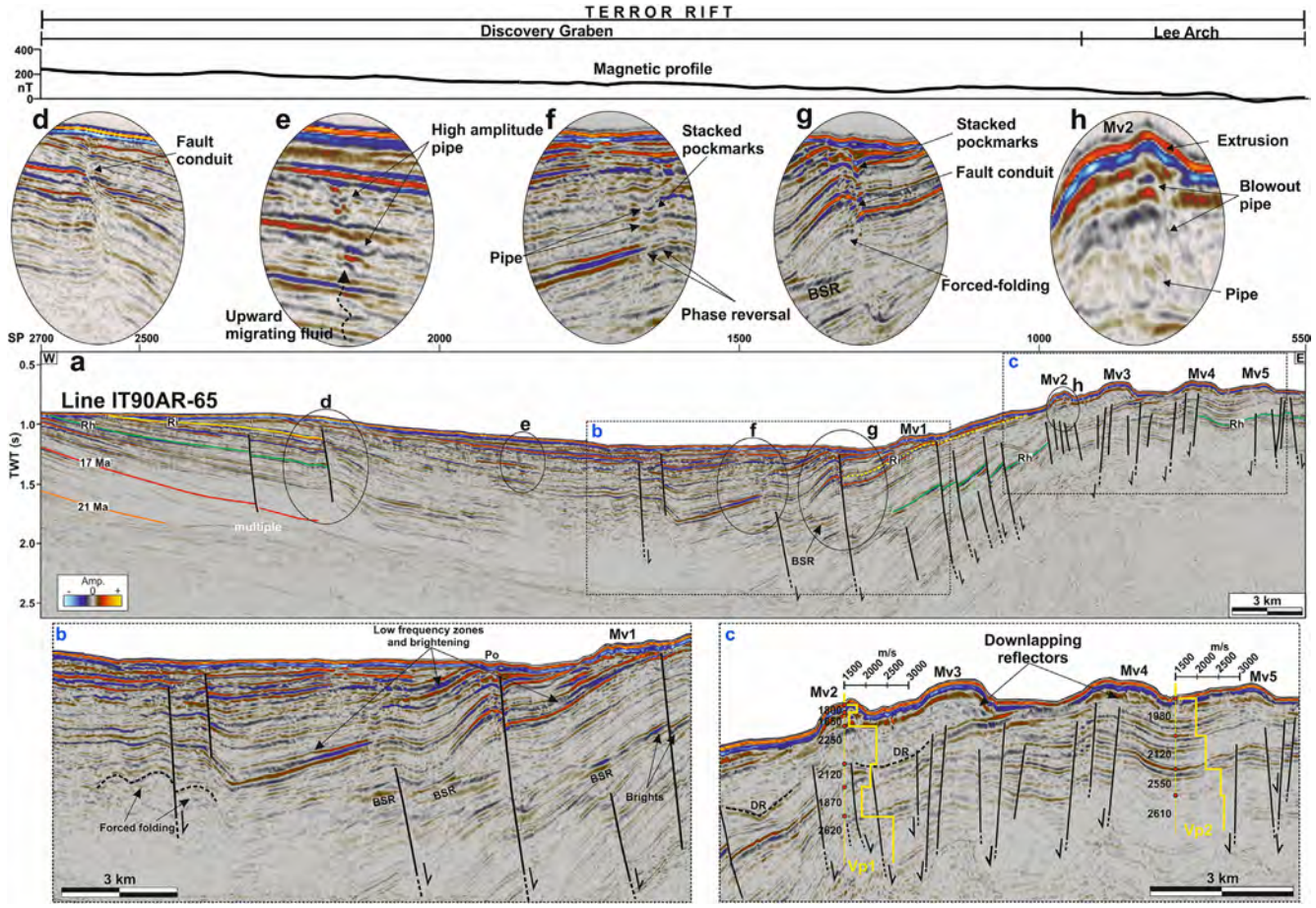

Fig. 4. Multichannel seismic line IT90AR-65 (see Figs. 1 and 3 for location), showing the occurrence of mud volcanoes (Mv) up to 1.5 km wide, lying on the Late Miocene erosive sea floor surface of Lee Arch. The seismic profile evidenced features related to fluid occurrence and migration: the Bottom Simulating Reflector (BSR) as the interface between gas hydrate above and free gas below (Fig. 4a, b, g); the Downdipping Reflector (DR) at the base of the Mv2 and Mv3, that represents an abrupt change of the interval velocities from 2250 m/s above to 1870 m/s below in Vp1, suggesting gas occurrence feeding the mud volcanoes, unlike the Vp2 with a normal velocity increment outside (Fig. 4c); fluid migration along fault conduits (Fig. 4d, g), high amplitude pipe (Fig. 4e) and blowout pipe feeding the mud volcano Mv2 (Fig. 4h); forced-folding due to fluid and mud intrusion (Fig. 4b, g); stacked pockmarks related fluids expulsion (Fig. 4g); low frequency zone, brightening (Fig. 4b) and phase reversal (Fig. 4f) related to gas bearing sediment. The magnetic profile by Gantar and Zanolla (1993) at the top of the figure does not show any significant anomalies at the mud volcanoes.

explosion (Cartwright and Santamarina, 2015). Seafloor pockmarks about 200 m large and buried and stacked pockmarks occur above fault conduits (Figs. 4 and 6). The crater of the diatreme is 2 km wide and 100 ms deep (nearly 75 m), is bounded on the west by the eject ring almost 1 km wide and about 30 m high, and to the east by the Mv10, Mv11, almost 200 m wide and 10–15 m high (Fig. 6). Underneath the diatreme there is a V-shape feature over 200 ms deep, that cuts subparallel reflectors, and contains chaotic and faint seismic facies (Fig. 6). The magnetic profile, collected along the seismic profile, by Gantar and Zanolla (1993) does not show significant anomalies in correspondence of the mud volcanoes (Fig. 6).

The morpho-bathymetric data show that the larger flat-topped mounds have a diameter of about 4000 m and a height of about 80 m with an asymmetrical NW-SE profile, with a south-eastward steep side with a slope between 21° and 24°, and a staircase morphology along the north-east side, which has a steep upper part (Fig. 7).

The top of the mounds shows a concentric pattern morphology, with rings few metres high made up of tens or even hundred metres wide cones (Figs. 7 and 9). The mounds are characterised by a transparent acoustic facies on the high resolution chirp data (Fig. 9c). The rings at the steep south-eastern external side have the highest relief and rimmed the mound (Figs. 3, 7 and 9).

On the Mv14 there are three pockmarks, two of them coalescent, are 40 m deep and about 50 m wide (Fig. 8).

The cone-shaped reliefs located along the eastern flank of the Discovery Graben in correspondence of fault strands (Figs. 3, 5 and 10) have been named Iulia and Tergeste mud volcanoes (SCAR Composite Gazetteer of Antarctica https://data.aad.gov.au/aadc/gaz/scar) by Geletti and Busetti (2011, 2022). The size of these features varies from the largest kilometre-scale Iulia Mud Volcano with a width of about 2500 m × 1500 m and a height of 40 m, to the Tergeste Mud Volcano with a width of about 750 m × 2000 m and a height of 35 m. Tergeste and Iulia are two elongated mud volcanoes (Figs. 5 and 10): morphological data show that they consist of a stack of conical mud volcanoes oriented roughly N–S. Details of the morpho-bathymetric data between the Iulia and Tergeste mud volcanoes show morphologies such as mud cones and gryphons (small mud outlets), pockmarks at their base and mud flows along their flanks (Figs. 8 and 10). They overlie reflectors characterized by the presence of the BSR. Target reprocessing provides detailed velocity profiles showing an average velocity of nearly 2000 m/s for these reliefs, and a velocity inversion for the underlying sediment of 1765 m/s, as well as a prominent velocity inversion from 2130 m/s to 1360 m/s in correspondence with a zone characterized by low frequency and high amplitude discontinuos horizons bounded by faults that cut

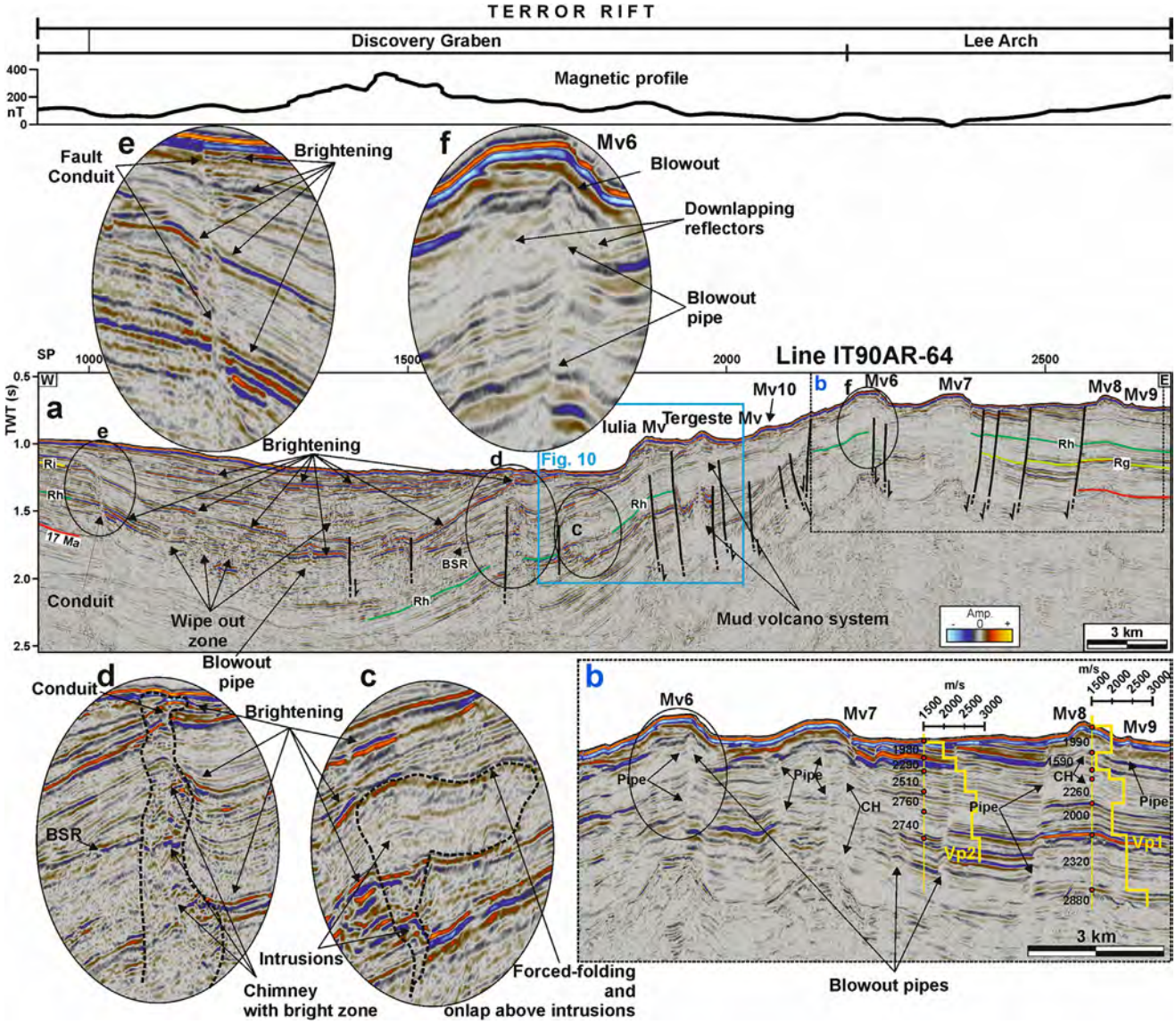

Fig. 5. Multichannel seismic line IT90AR-64 (see Figs. 1 and 3 for location), showing the occurrence of mud volcanoes (Mv) up to 2 km wide, lying on the Late Miocene erosional sea floor surface of Lee Arch. Iulia and Tergeste mud volcanoes (SCAR Composite Gazetteer of Antarctica, https://data.aad.gov.au/aadc/gaz/scar) were identified by Geletti and Busetti (2011; 2022). The seismic profile shows evidence of features related to gas/fluid occurrence and migration: the Bottom Simulating Reflector (BSR) as the interface between gas hydrate above and free gas below interrupted by a wide bright zone chimney (about 500 m) (Fig. 5a, d); wipe out zone with disrupted reflectors (Fig. 5a); pipes and blowout pipes associated with upward migration of gas/fluid and feeding the mud volcanoes (Fig. 5b, f); fault conduits with brightening horizons due to gas occurrence (Fig. 5e); forced-folding associated with fluid/mud intrusion with onlap of the above horizons (Fig. 5c). Velocity profile Vp1 through the Mv8 shows velocity inversion below the base of the Mv from 1990 m/s to 1590 m/s indicating gas bearing sediment below; the velocity profile Vp2 through the sedimentary sequence shows no abrupt inversion (Fig. 5b). The magnetic profile by Gantar and Zanolla (1993) in the upper part of the figure, shows no significant anomalies in correspondence of the mud volcanoes.

through the BSR. The free gas-bearing sediments below the BSR are the primary source of the gas, and zones of low amplitude reflections such as the blowout pipes and conduits along faults are the fluid pathways from the sediment below the BSR to the Mvs. Intrusion of possible mud and fluids gives rise to deformation of the intruded sediment into arc geometries. Indications of gas occurrences in the sediment are provided in the migrated MCS by the low frequency zone with bright horizons, and by the high amplitude and low frequency zones below the MVs in the instantaneous amplitude or magnitude section (often referred to as "trace envelope" or "reflection strength") and the instantaneous frequency section, respectively (Fig. 10).

In area B, a single cone-shaped relief (Mv19) nearly 4000 m × 4000 m wide and 100 m high occurs on the western side of the Lee Arch towards the Discovery Graben, at a depth of about 750 m (area B in Fig. 1; Fig. 11). The chirp profile shows transparent lenses, probably a debris flow and the associated scar above, and a depression on the flank, probably a crater. Similarly, the morphological data show the same features.

The Mv19 overlies sediment post RSU4, which is of Middle Miocene age. RSU4 is displaced by faults with several hundred metres of offset. These faults bound forced folds: the central one is connected to the Mv19 surface by conduits, while the two forced folds north and south of the Mv19 respectively, produce positive seafloor morphologies, and they are all associated with the occurrence of chimneys, conduits, pipe and blowout pipes (Fig. 11).

In area C, located offshore the Adare Peninsula in the northernmost continental margin of the Ross Sea (Fig. 1 for location), IBSCO

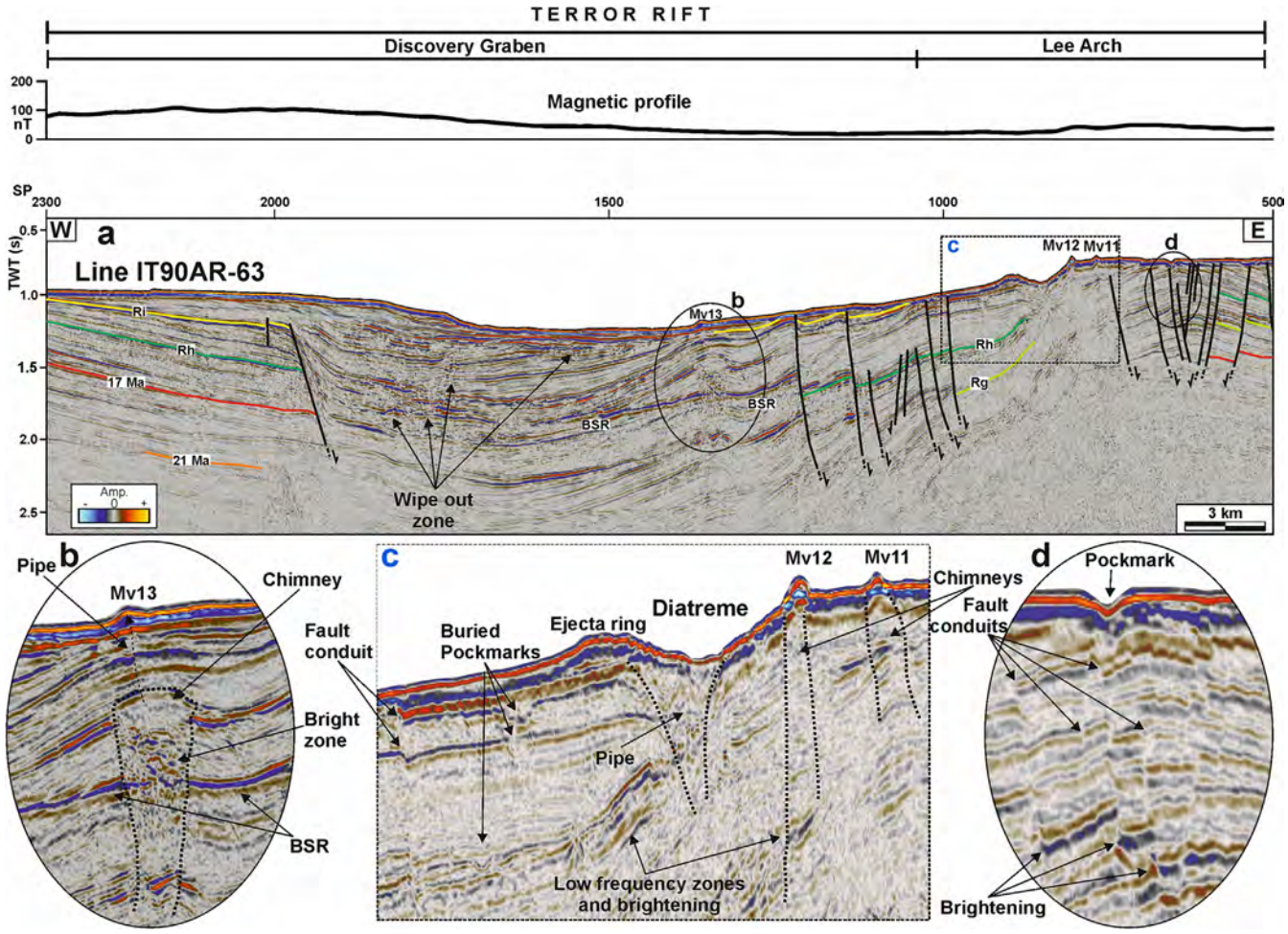

Fig. 6. Multichannel seismic line IT90AR-63 (see Figs. 1 and 3 for location), shows evidence of features related to gas/fluid occurrence and migration: small mud volcanoes (Mv10, 11 and 12) lying at the border of a 2 km wide diatreme crater with the ejecta ring and the underlying V-shape conduit (Fig. 6a, c); the Bottom Simulating Reflector (BSR) as the interface between gas hydrate above and free gas below (Fig. 6a, b) interrupted by a nearly 1 km wide chimney marked by a bright zone associated with gas occurrence, and feeding the Mv13 (Fig. 6b); fault conduits below a pockmark (Fig. 6d); buried pockmarks near the giant pockmark (Fig. 6c); wipe out zone and low frequency zone associated with the gas presence (Fig. 6a, c). The magnetic profile by Gantar and Zanolla (1993) show no significant anomalies.

morpho-bathymetric data (Dorschel et al., 2022) show several cone-shaped reliefs (Fig. 12a) on the continental shelf at about 600 m of water depth, some of which are crossed by the seismic profile BGR80-100 (Barro Savonuzzi et al., 2023), (Fig. 12b, c). The largest relief Mv22 is about 5000 m in diameter and 300 m high, and Mv21 is about 2.5 km wide and 100 m high. The seismic profile BGR80-100 shows that the reliefs are characterised by internal low amplitude, discontinuous reflectors downlapping on a high-amplitude horizon with upward convexity. The velocity field calculated on the seismic profile BGR80-100 (Barro Savonuzzi et al., 2023), shows that the reliefs have a velocity of 2100 m/s, and Mv22 lies on a body with velocity of about 2700 m/s (Fig. 12c). A NE dipping high-amplitude reflector from 1.75 s to 2.00 s, disappears below the mounds due to kilometre wide chimneys with low amplitude and chaotic reflections inside causing a forced tilting of the lateral sedimentary sequences. Pipes connect the chimneys to the mud volcanoes, and Mv21 shows a V-shaped top, probably a crater (Fig. 12b, c).

4.2. The buried reliefs in the Northern Basin and Roosevelt sub-basin

The buried reliefs are located on the western flank of the Northern Basin (northwestern Ross Sea), (area D in Fig. 1), and in the Roosevelt sub-basin (southeastern Ross Sea) (area E in Fig. 1).

Some of the buried reliefs in the northwestern Ross Sea are crossed by the MCS profile IT88A-06 (Fig. 13). The buried reliefs are located where the seafloor is between 450 m and 600 m deep. They overlie the RSU4, dated at Middle Miocene in age (14.6–15.8 Ma), while their top has been correlated to the Early Quaternary RSU2 by Brancolini et al. (1995). These morphologies are sealed by about 250–450 m (velocities from 1900 m/s to 2400 m/s) of Quaternary glaciomarine sediments. The largest reliefs have a symmetrical dome-shape with a flat top, while the smaller ones have a conical shape (Fig. 13). The height of the reliefs varies considerably from about 60 ms to over 280 ms, which corresponds to about 90–400 m (considering an internal velocity of about 3000 m/s), and the width varies from a few hundred metres to about 9 km. The reliefs are close to each other (generally the distance is a few kilometres) and some of them merge together.

The seismic facies of the buried reliefs is characterised by an alternation of parallel convex reflectors with low to high-amplitude. In the time profile the seismic sequence beneath the reliefs appears generally well-stratified (Fig. 13a). The reflectors inside the reliefs show downlap terminations on subhorizontal horizons with pull-up effect in the time domain, indicating a strong acoustic impedance contrast between the reliefs succession and that of the surrounding sediments, while the depth migrated

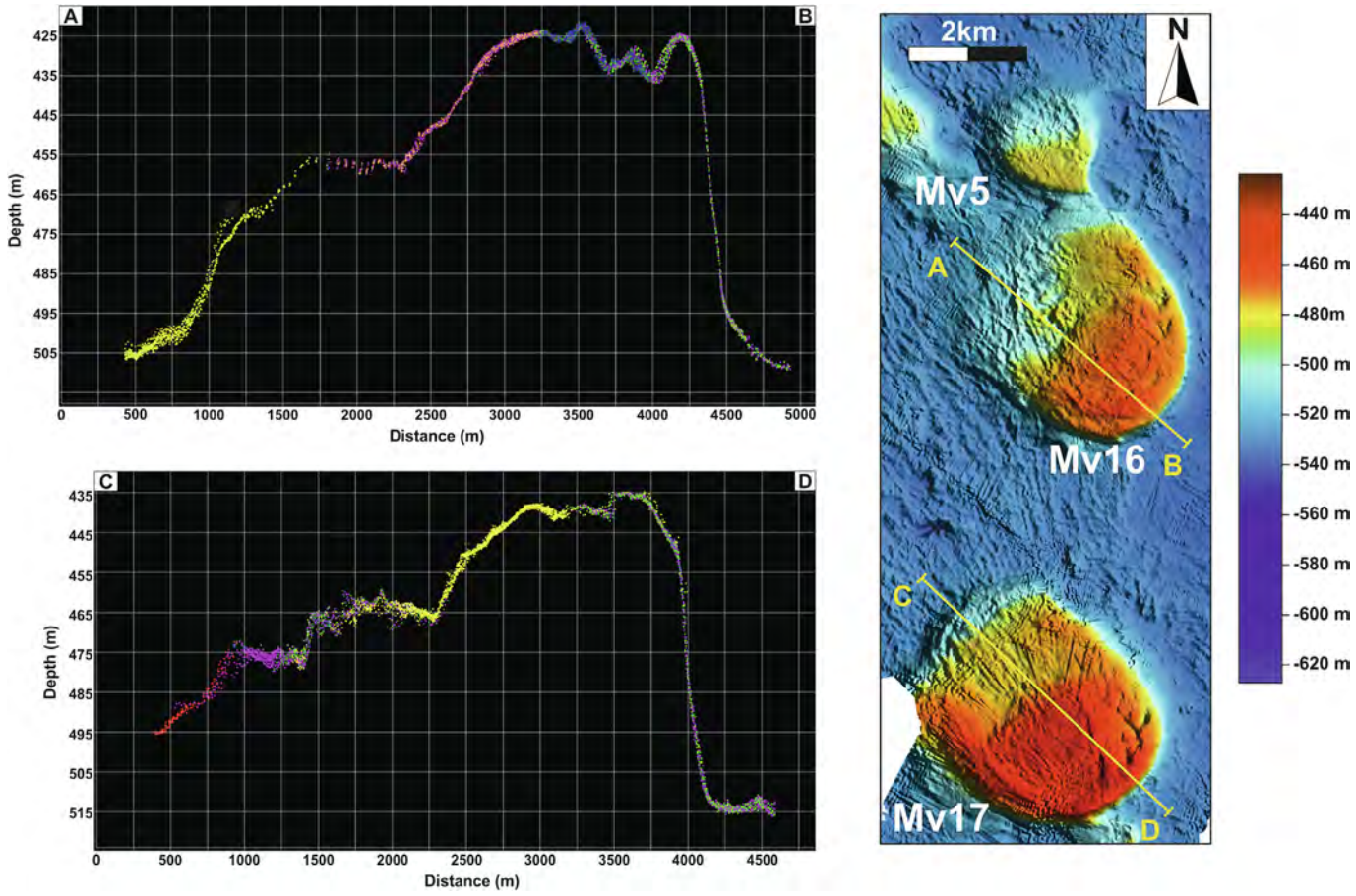

Fig. 7. NW-SE morpho-bathymetric profiles showing the shape along the maximum axis of the Mv16 and Mv17 (see Fig. 3 for location). They present a maximum extent of about 4000 m, a steep south-east side with slope between 21° and 24°, and a staircase morphology along the north-east side that shows a main steep upper part. The subcircular top is characterized by an undulated morphology, with a rimmed south-east border.

profile shows that the horizons at the base of the reliefs are sub-horizontal (Fig. 13).

The seismic velocity analysis shows a velocity range from 2700 m/s to 3140 m/s for the reliefs, and from 1900 m/s to 2400 m/s for the Quaternary sediment sealing the reliefs. Below the reliefs the velocity is about 3200 m/s.

The blanking seismic facies below the relief and the occurrence of chimneys, pipes and bright zones indicate the presence of a fluid system feeding the mud volcanoes.

The buried reliefs in the Roosevelt sub-basin are imaged by the NBP-0301-27B multichannel seismic line. They appear as seven buried reliefs in an area between 700 m and 900 m water depth (Barro Savonuzzi et al., 2023) (Fig. 14). They are of similar size and shape, up to 150 m high and up to 5000 m wide, and their tops lie between a few metres and 150 m below seafloor. The mounds lie on a laterally discontinuous, irregular high-amplitude reflector overlying the Middle Miocene RSU4, and some of them are truncated at the top by an erosional unconformity. The internal seismic facies of the mounds is characterised by faint, downlapping to chaotic reflectors. The reliefs are onlapped and draped by sub-horizontal reflectors with low amplitude and medium lateral continuity. Locally, these reflectors are dipping or pinching toward the mounds (Fig. 14). The reliefs are characterised by relatively high velocity anomalies, ranging from 2600 m/s to 3000 m/s, higher than the velocity of the seismic section below them, being about 2000–2400 m/s. A local amplitude reduction produces acoustic blanking beneath the mounds, interrupting the lateral reflectors continuity, including regional unconformities RSU4 and RSU5 (Fig. 14b), probably related to the presence of gas chimneys, with horizons characterised by a pull-up effect on the lateral reflectors. The areas with low amplitude, interpreted as chimneys, are about 500 m wide and extend vertically for several hundred metres.

5. Discussion

Seafloor and buried morphologies detected on the Ross Sea continental margin can occur both in clusters and as isolated reliefs. The analyzed reliefs are found to have similar sizes, being few kilometres wide and up to tens of metres high. Their internal seismic facies may present as either oblique and faint reflectors or chaotic reflectors. The mounds generally lie on a well-stratified sedimentary succession.

The seafloor reliefs of the study area A have previously been considered as magmatic volcanoes by Cooper et al. (1987) and Brancolini et al. (1995), and more specifically as tuyas, subglacial flat-topped volcanoes by Lawver et al. (2012), while Greenwood et al. (2018) defined their morphology as sedimentary wedges pinned on seamounts, recording a retreat of the ice grounding line.

For the buried reliefs (area C) the most plausible origin was attributed to volcanism by Boehm et al. (1993), and for those of the Roosevelt sub-basin (area D) to a morainic origin (Sorlien et al., 2007).

In this work, further analysis of the seismic data compared to the original profiles from the early 1990 s (e.g. Boehm et al., 1993; Geletti et al., 1993) has provided a more detailed picture of the acoustic facies associated with the mounds through

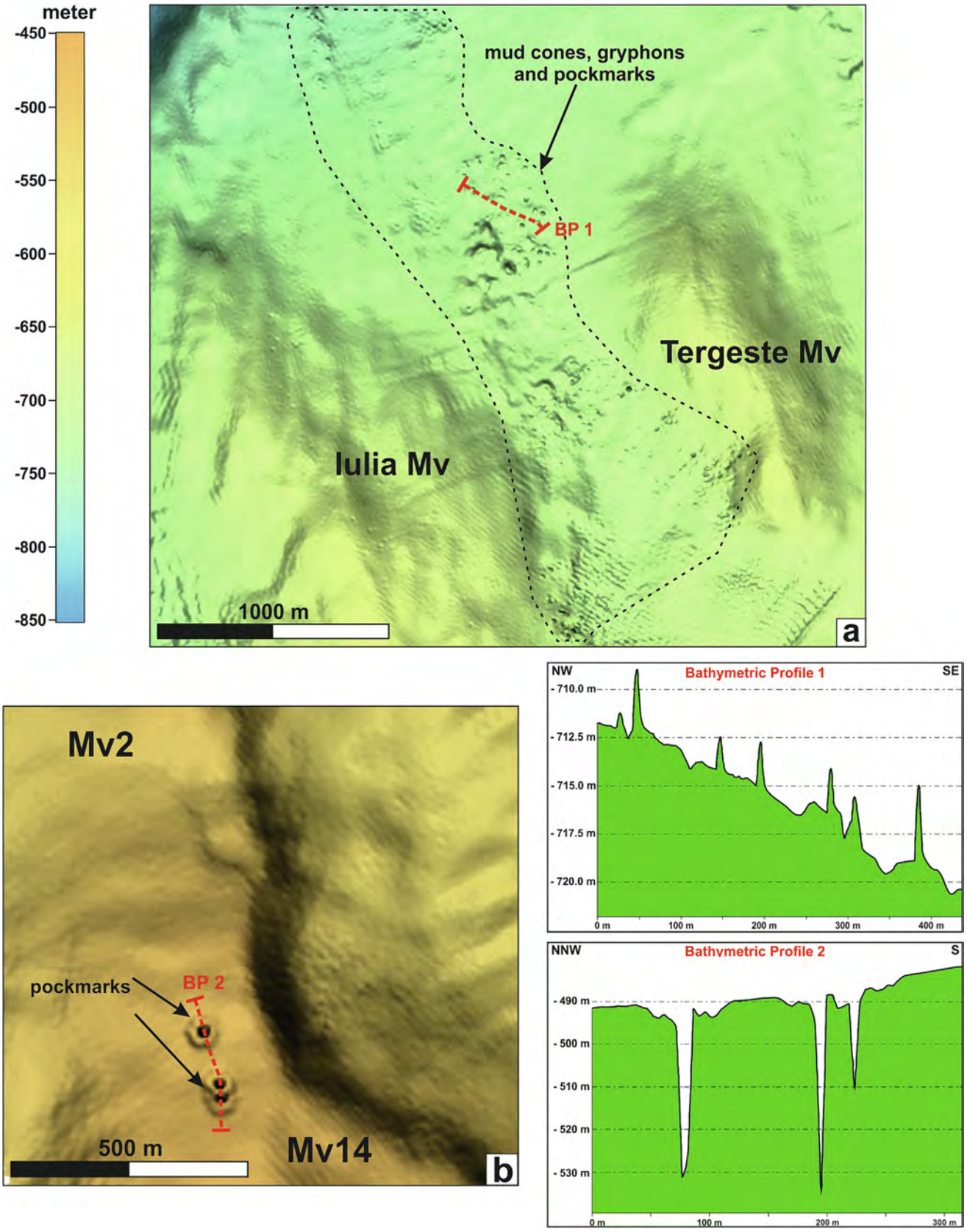

Fig. 8. Details of the morpho-bathymetric data of the OGS Explora Mounds (see Fig. 3 for location): (a) field consisting of mud cones, gryphons up to 4 m high, and pockmarks between the Tergeste and Iulia mud volcanoes (see BP1) indicating recent activity; (b) three pockmarks about 50 m wide, two of them merging together, located on the top of Mv2 (see BP2).

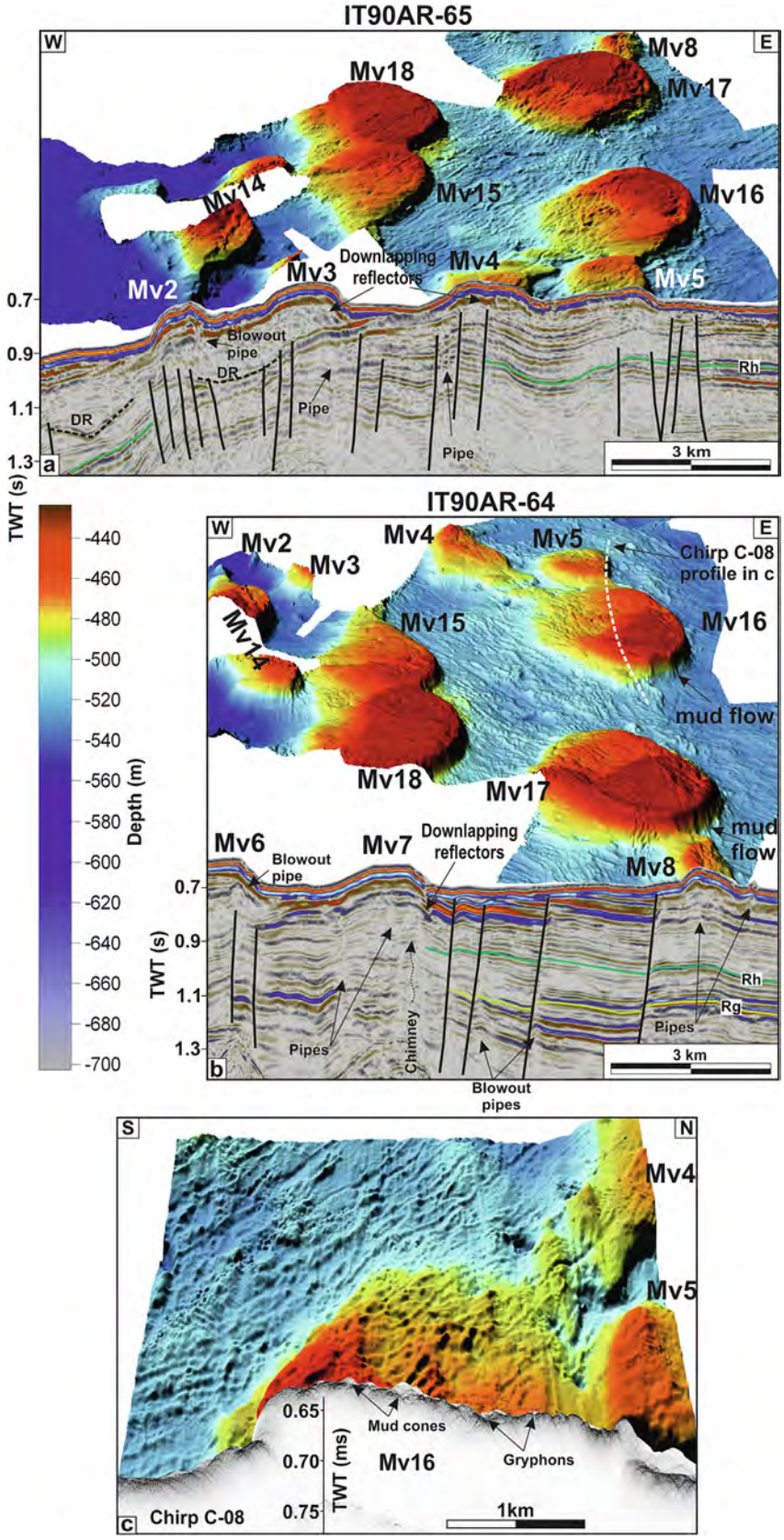

Fig. 9. Association between seismic and OGS multibeam data (see Fig. 3 for location): (a,b) the OGS Explora Mounds imaged by the multichannel seismic profiles (reported in Figs. 4 and 5) present the same acoustic facies (low amplitude, chaotic and downlapping seismic horizons, with occurrence of pipes and blowout pipe) and morpho-bathymetric features indicating their mud volcanic origin; (c) the chirp profile C-08 and the morpho-bathymetric data show the complex top morphology of the Mv16 associated with the presence of mud cones and gryphons.

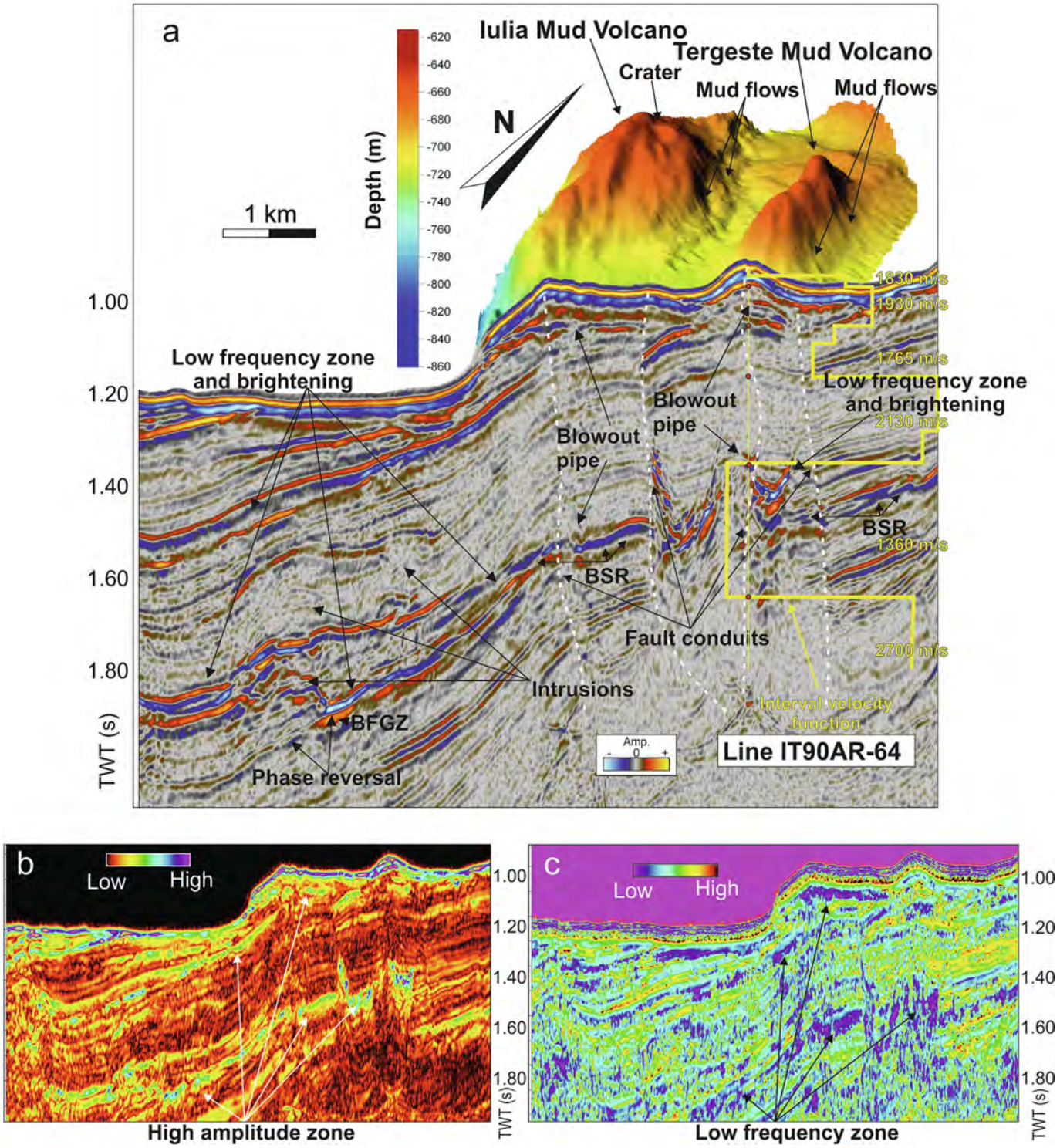

Fig. 10. Iulia and Tergeste mud volcanoes and related gas plumbing system located in the eastern sector of the Discovery Graben (see Fig. 3 for location): (a) morpho-bathymetric data evidence the roughly north–south elongated shape of the mud volcanoes associated with faults: the Tergeste is composed by three main cones, while the Iulia consists of a ridge with a main central body with a crater on the top, both the MVs with mud flows draping the flanks. Part of the multichannel seismic profile IT90AR-64 (see Fig. 5), modified after Geletti and Busetti (2011, 2022), showing acoustic evidences of gas occurrence and migration such as the Bottom Simulating Reflector (BSR), the Base of the Free Gas Zone (BFGZ), the low frequency zone and brightening disrupted horizons close to fault conduits and blowout pipes indicating fluid migration feeding the mud volcanoes; (b) reflection strength section evidence the high amplitude zone below the mud volcanoes related to gas occurrence as shown also in (c) by the instantaneous frequency section with low frequency zones.

reprocessing. The results show that the seismic facies differ from that of a volcano, with no signs of magmatic intrusions. Additionally, the sedimentary succession in the area surrounding the mounds is well-preserved. Volcanic features in the western Ross Sea are clearly evident on the seismic data (Cooper et al., 1987), as for the seafloor lava cones as well as for the unstratified acoustic facies beneath the cones due to magmatic conduits and thermal metamorphism.

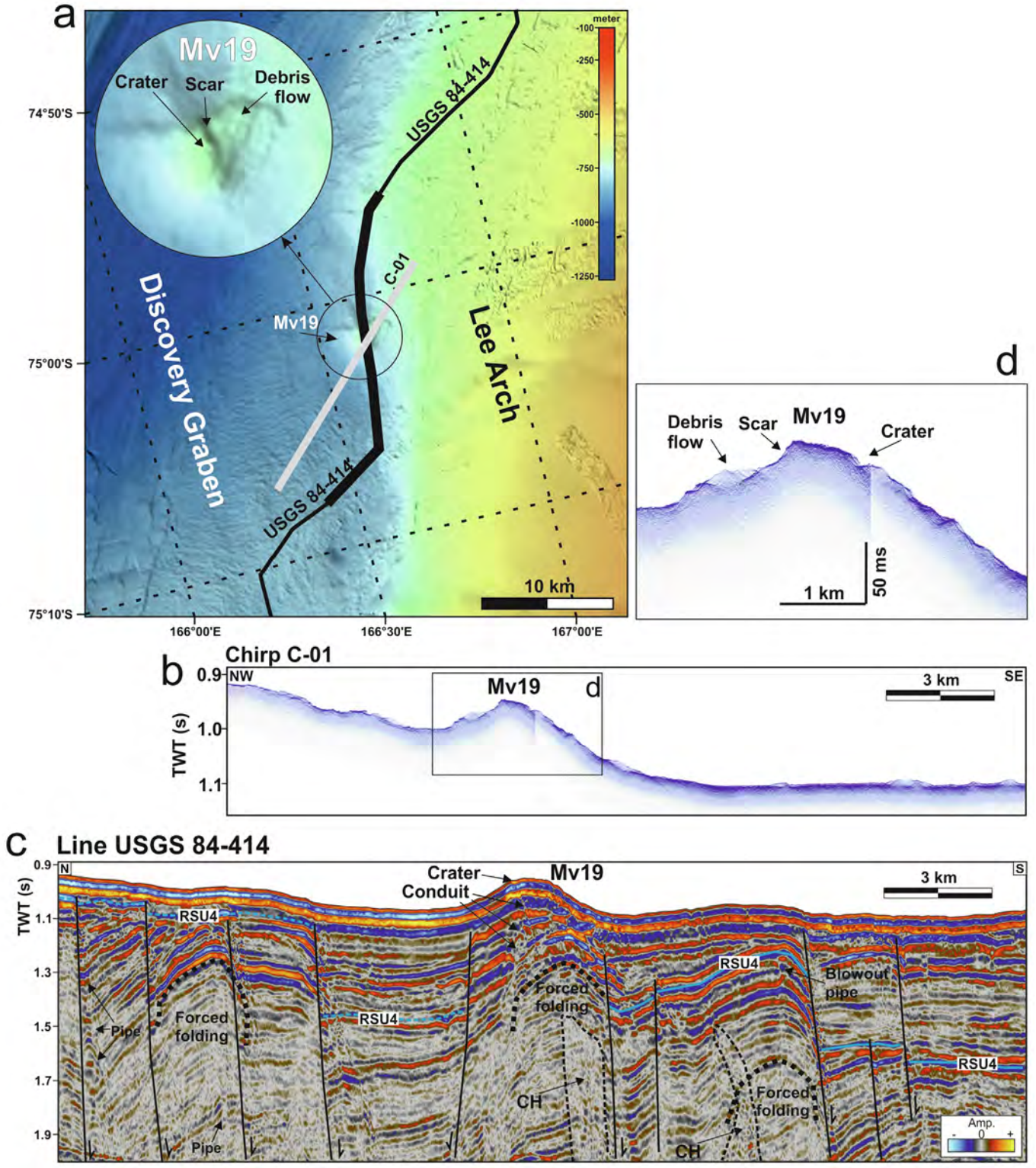

Fig. 11. The mud volcano (Mv19) identified in the study area B (see Fig. 1 for location): (a) morpho-bathymetric map produced by merging low resolution IBCSO data (Dorschel et al., 2022) with high resolution OGS multibeam data, showing the Mv19 that is about 100 m high and 4000 m × 4000 m large; (b) the migrated chirp profile evidences the cone shape morphology of the MV19 characterised by a crater and a possible mud cone on the flanks; (c) the multichannel seismic profile USGS84-414 shows the Mv19 feeded by a gas plumbing system characterised by conduits and chimney underneath a forced fold; (d) zoom of chirp profile with evidence of Mv with crater, debris flow and scar. Other chimneys, and forced folds producing positive seafloor morphologies, are present.

The McMurdo Volcanic Group is located in Victoria Land and the western Ross Sea and was first documented by LeMasurier et al. (1990). The volcanic activity of the McMurdo Group has a history ranging from the Miocene to the present, and includes active volcanic centres such as Erebus and Melbourne, as well as volcanic islands such as Ross and Franklin Islands and several seamounts (Fig. 1). It belongs to the Cenozoic alkaline volcanic province related to the West Antarctic Rift System (Behrendt et al.,

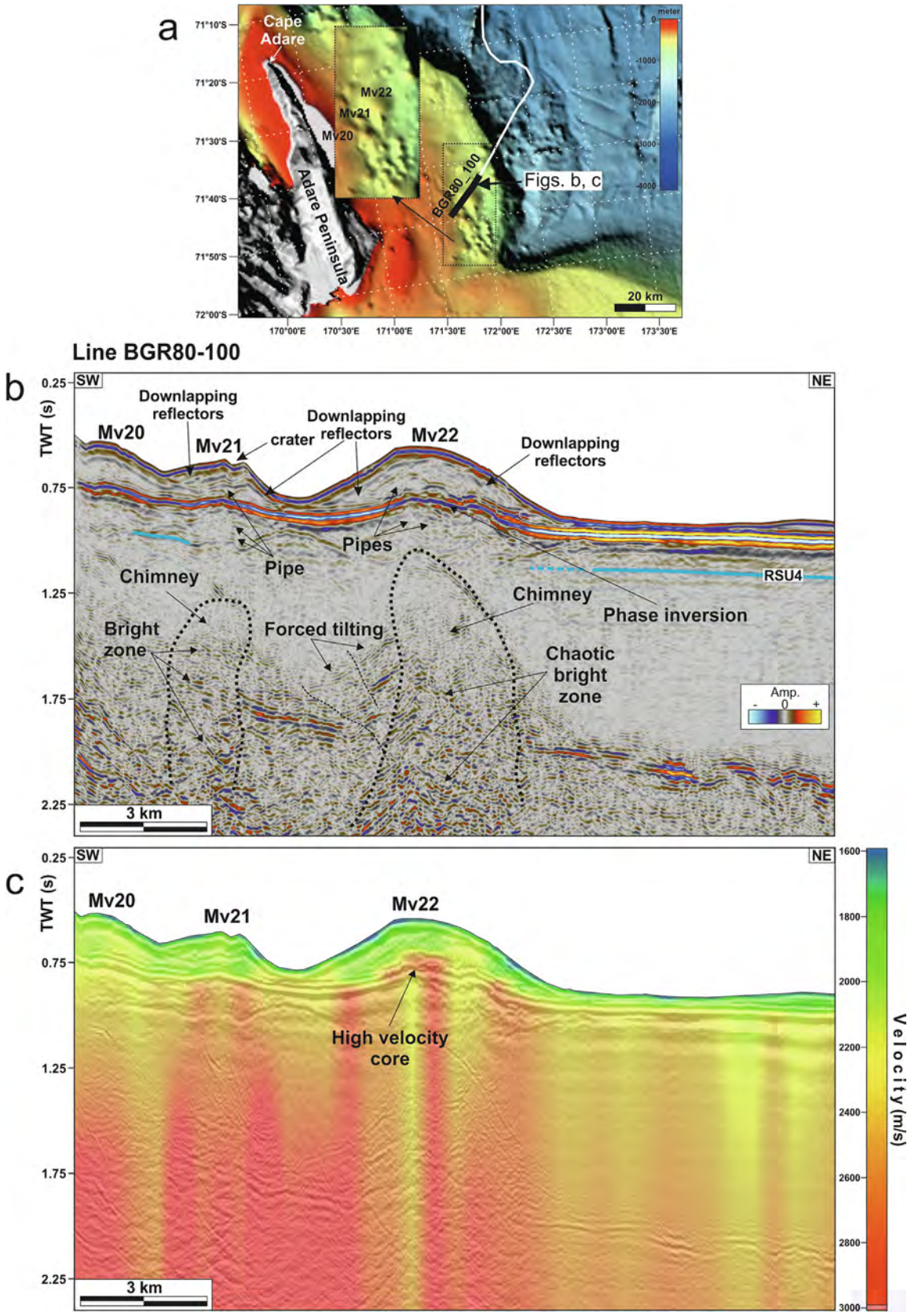

Fig. 12. Mud volcanoes in the study area C, offshore Adare Peninsula, (see Fig. 1 for location): (a) morpho-bathymetric map from IBCSO (Dorschel et al., 2022) showing the presence of a field composed of cone shape reliefs on the continental shelf (see blowup); (b) multichannel seismic profile BGR80-100 (modified after Barro Savonuzzi et al., 2023), evidences Mv22 about 5000 m wide and 300 m high, Mv21 about 2000 m wide and 100 m high with a depression on the top, possibly a crater, both with internal discontinuous reflectors downlapping on a very high amplitude reflector. Moreover, two areas with chaotic, discontinuous, low amplitude reflections, interpreted as chimneys, about 1 and 3 km wide respectively, with bright zones inside, feed the mud volcanoes through pipes. Forced tilted bright horizons are visible at the side of the chimney below Mv22; c) the velocity field shows that the Mv22 has a medium–low velocity of 2100 m/s with a high velocity core of approximately 2700 m/s.

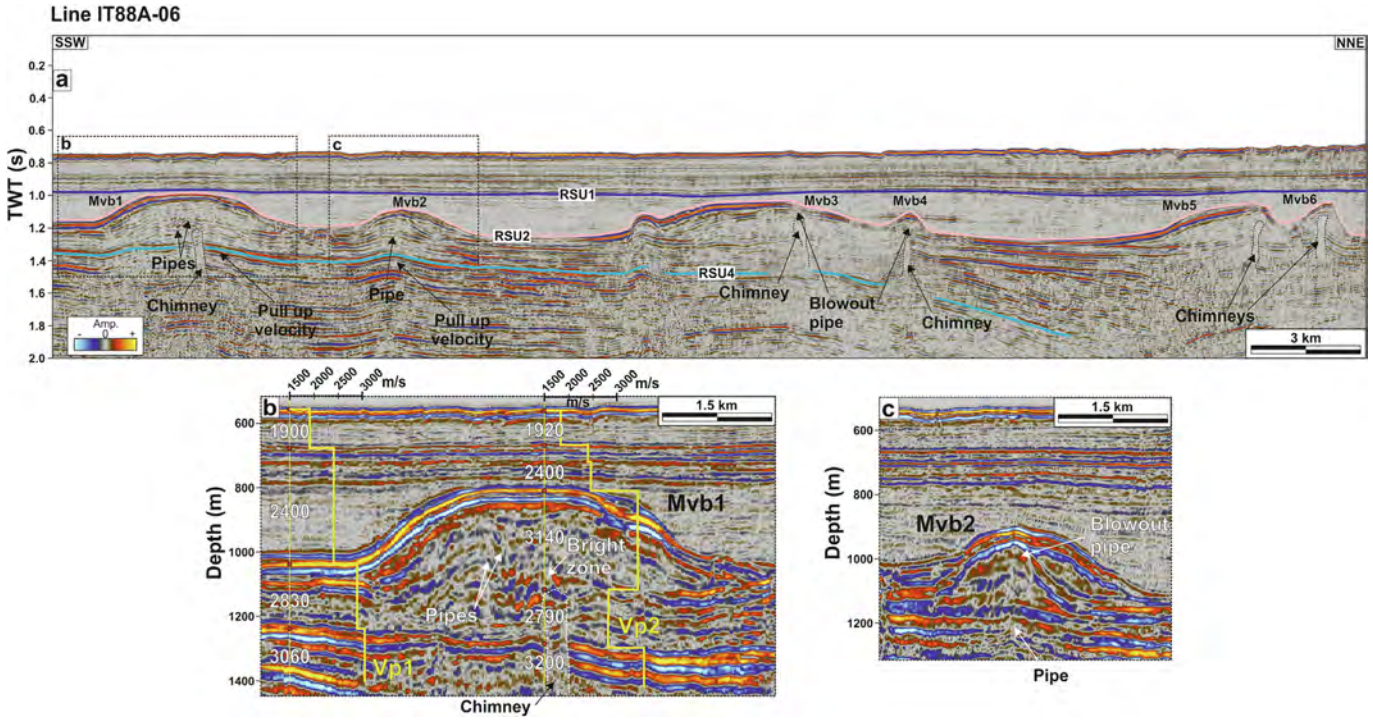

Fig. 13. Buried mud volcanoes (Mvb) identified in the study Area D in the Northern Basin (see Fig. 1 for location): (a) multichannel seismic profile IT88A-06 showing possible buried mud volcanoes up to 6000 m wide and 300 m high, with faint oblique horizons, overlying the Middle Miocene RSU4 and covered by Quaternary sediment onlapping above RSU2; (b) the depth migrated profiles across Mvb1 and Mvb2 show the real geometries of the horizons with flattening the velocity pullup effect, and the velocity function Vp1 shows high velocities of 3140 m/s overlying a velocity inversion of 2790 m/s which interface coincide with the bright zone in the core of Mvb1. The presence of the acoustic blanking facies, from which chimneys and pipes rise, indicates the presence of a plumbing system feeding the mud volcanoes.

1991). The McMurdo Volcanic Group in the Northern Victoria Land presents the highest amplitude aeromagnetic anomalies, up to –500 nT (Ferraccioli et al., 2009), and the volcanic cones near Franklin Island are also associated with high magnetic anomalies of up to 300 nT (Rilling et al., 2009). Conversely, the reliefs in the western Ross Sea do not have such a high magnetic anomaly, and four of them have a small normal magnetic anomaly of about 50–100 nT (Lawver et al., 2012).

Therefore, a potential magmatic origin for the western Ross Sea reliefs would not be supported by the available aeromagnetic data.

Based on the seismic evidence from the target processing of the MCS and Chirp profiles, the morpho-bathymetric data, and the presence of the already known Iulia and Tergeste mud volcanoes (Geletti and Busetti, 2011, 2022), we propose that the other studied reliefs are also mud volcanoes.

In this section, the origin of the reliefs as mud volcanoes is discussed, considering them as the expression of a cold seep system composed by source rocks, plumbing system and seafloor morphologies, or due to mud mobilisation by gravitative instability of the clayey sediment and fluid overpressure.

5.1. The source rock

In the whole Ross Sea, the sedimentary units feeding the Mvs are Miocene or older. In the western Ross Sea, in area A, the sedimentary units feeding the Mvs are at least older than the Late Miocene Rh unconformity, and possibly older than the Middle Miocene Rg unconformity. In all other study areas, the Mvs are fed by sedimentary units older than the Middle Miocene RSU4 or even older than the Early Miocene RSU5 in the Roosevelt sub-basin.

The sedimentary units in the Ross Sea document the Cenozoic rift phase with the transition from Early Cenozoic continental to Middle–Late Cenozoic marine environment and influenced by the establishment of an ice sheet with expansion and decay of ice streams in the Antarctic continent since Late Eocene (Fig. 2). Consequently, since the Middle Cenozoic, sedimentary sequences have consisted of an alternation of marine sediments mainly composed by lithified or semi-lithified silty clay and mudstone, and glacial-marine sediment composed mainly by diatom-bearing/rich mudstone with the presence of ice rafted debris. All of these lithologies may contain organic matter, although the hydrocarbon content of these sequences from the drill sites (as described in section 2.1) generally indicates low content for Pliocene sediments and a slight increase in content in the Miocene–Eocene sediment (Fig. 2). Even small amounts of gas are known to produce seismic amplitude anomalies (Taner et al., 1979), and in the Ross Sea the geophysical data indicate frequent acoustic anomalies related to the presence and migration of gas.

5.2. The plumbing system

The geophysical evidence for the presence of gas hydrate and free gas has already been recognized by Geletti and Busetti (2011) in area A (OGS Explora Mounds), and consists of different types of high amplitude reflectors such as the Bottom Simulating Reflectors (BSRs), the Cross Cutting Reflectors (CCRs) and the Enhanced Amplitude Reflectors (EARs). Modelling of the gas hydrate equilibrium according to the curve of Sloan (1990) is consistent with a gas composition consisting mainly of methane (Geletti and Busetti, 2011).

Acoustic anomalies, such as low frequency zone and bright horizons, phase reversal, wipeout zone, as well as seismic velocity inversions, clearly indicate the occurrence of gas bearing sediment. The gas migrated through pathways as chimneys, pipes and fault conduits that feed the mud volcanoes. The above mentioned different types of acoustic anomalies are more common in the areas A, B and C where the Mvs lie on the seafloor, respect in the area D and E with the buried Mvs.

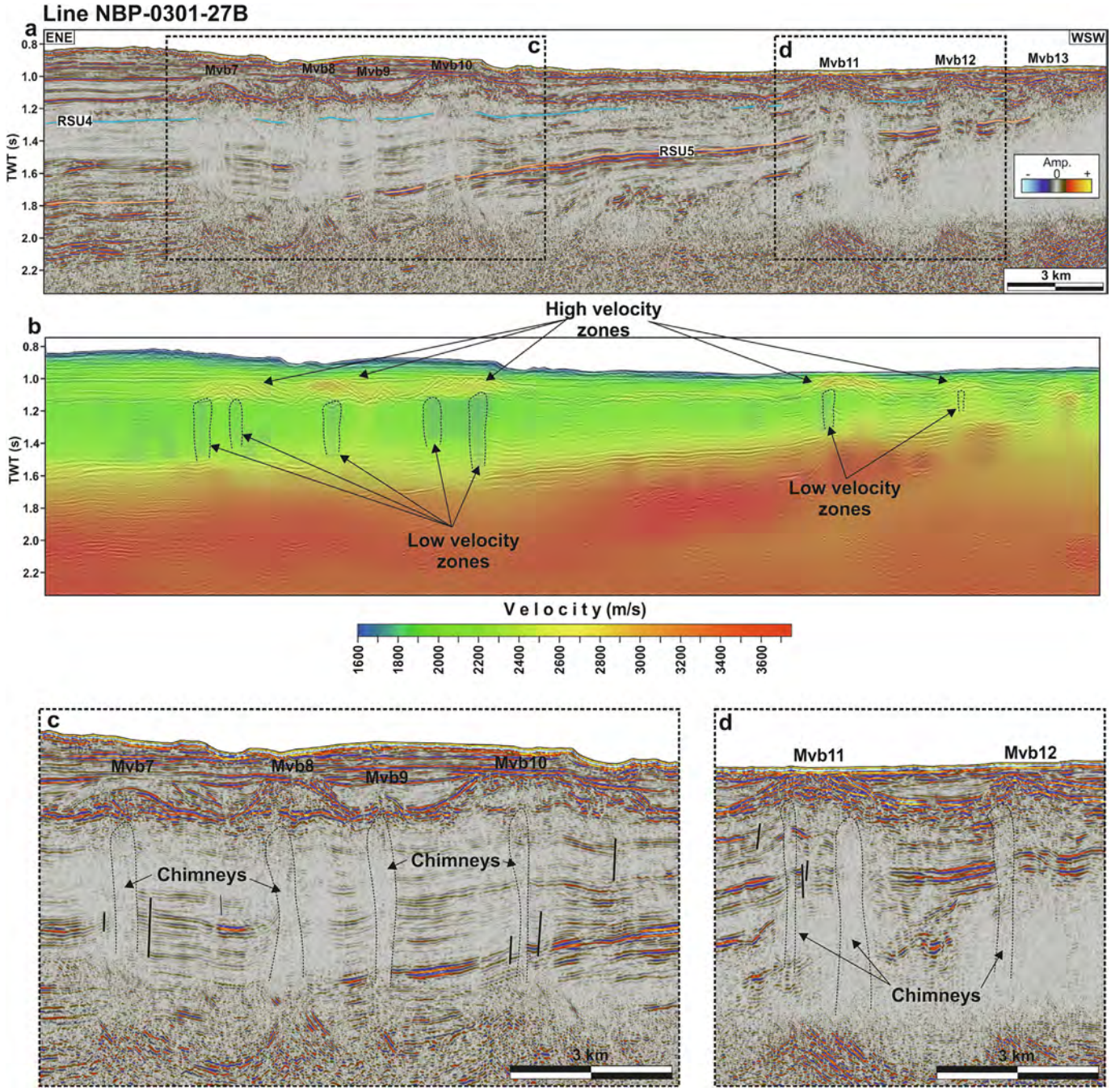

Fig. 14. Buried mud volcanoes (Mvb) identified in the study area E in the Roosevelt sub-basin (see Fig. 1 for location): (a) multichannel seismic profile showing possible buried mud volcanoes up to 3000 m wide and about 200 m high, overlying the Middle Miocene RSU4 (modified after Barro Savonuzzi et al., 2023); (b) velocity field showing the high velocity zones coincident with the Mvbs, and the vertical low velocity zones below corresponding to the chimneys (Fig. 14c, d), which together with the acoustic blanking facies and the pipes indicate the presence of a plumbing system feeding the mud volcanoes.

In area A, the gas mainly derives from the free gas-bearing sediments below the gas hydrate layer, and migrates upward through seepage pathways that cut through the stratigraphic succession down to the BSR. Tectonic control seems crucial in driving fluid migration. In fact on the N–S Lee Arch, some km wide anticline dissected by N–S trending sub-vertical faults locally affecting the seafloor (Cooper et al., 1987; Sauli et al., 2021), tectonic control on the nucleation of the mud volcanoes seems to be significant as they are aligned along the faults bounding the eroded structural highs.

Forced folding of the sedimentary sequence formed near or between faults, as occurs in areas A and B, may be due to upward migration of fluids and mud mobilisation processes due to gravity instability and fluid overpressure (Figs. 4, 5 and 6). Some forced folds are connected to the Mv through chimneys.

In fact, gas migration is not the only element responsible for mud mobilisation, and the mud diapirism and mud volcanism may be the result of a combination of gravitational instability of the clayey sediment and fluid overpressure (Kopf, 2002; Revil, 2002). Gravitational instability is caused by clayey sediments that have a density lower than that of the surrounding units, and rise by buoyancy, supported by the fluid overpressure and hydrofracturing (Mazzini and Etiope, 2017). Clayey components in the sediment are common in marine and in glacio-marine sequences of the Ross Sea. The overpressure condition could result from rapid deposition

of glacial sediment and glacial loading (Wangen 2022). In the Amundsen Sea (Antarctica), columnar acoustic features with poor reflection/blanking between 50 m and 500 m wide, have been interpreted as mud diapirs from water-rich sediment, without evidence of gas occurrence (Weigelt et al., 2012). During periods of ice sheet advance and grounding over the continental shelf, subglacial sediments are deposited above glacial marine sediments. Glacial marine sediments generally have a high water content, while subglacial sediments are generally highly compacted and have low porosity. If glacial marine sediments are rapidly covered by subglacial sediment, they could be pressed out (Weigelt et al., 2012). The presence of glacial marine sediments alternated with subglacial sediments in the Ross Sea, may be therefore a preconditioning factor for buried clay-rich layer overpressure, which could feed mud volcano systems.

The tectonic setting can favour the migration of fluid and sediment along the fault systems, as in the Lee Arch (areas A and B). In other areas where there is no clear active faulting and the acoustic anomalies related to gas bearing sediment are less evident, such as the Roosevelt sub-basin (area E) and in the areas C and D in the western Ross Sea, the development of mud volcanoes is likely due mainly to the buoyancy effect of clayey sediment. In area D and E the lack of mud volcanoes on the present sea floor may suggest that the conditions for gas accumulation, upward migration and mud expulsion ceased before the burial of the reliefs.

5.3. Seafloor morphologies related to gas/fluids and mud expulsion

Mud volcanoes have different morphologies that reflect the mechanism of eruption and erosion, and have been classified into twelve types by Mazzini and Etiope (2017). Different types can occur in the same province, for example in Azerbaijan, one of the largest mud volcano provinces in the world (Mazzini and Etiope 2017; Odonne et al., 2021).

Tergeste and Iulia are both N–S elongated mud volcanoes composed by the merge of several volcanic centres, oriented in a N–S direction that coincides with the Lee Arch fault system, indicating that the tectonic control is crucial in driving the fluid migration.

Morphologies such as mud cones with craters and gryphons, and mud flows are present (Figs. 8 and 9), suggesting that at least some mud volcanoes are still active (e.g., Iulia and Tergeste Mv, and Mv8). In area B, the mud volcano on the seafloor and the positive morphologies of the seafloor above the forced folds, indicate that up-ward fluid migration has been active in recent times.

The flat-topped mound can be considered as the plateau-like mud volcano of Mazzini and Etiope (2017), with relatively low elevation, steep and narrow flanks and the crater lying in a large plateau. Their ring-like structure is considered typical of the wide craters in which viscous mud breccia erupts intermittently, with the gradual collapse of the crater preventing growth at significant altitudes (Mazzini and Etiope 2017). The OGS Explora Mounds have ring geometries, with a plateau characterised by an outer ring that bounds the crater depression where a morphological high, probably constituted by mud breccia, may be locally present. Gryphons are disseminated within the mounds, especially along the outer rim, where mudflows occur, with evidence of overspilling (Fig. 9).

The occurrence of conical/elongated Mvs along the flank of the Discovery Graben and of subcircular flat-topped Mvs on the Lee Arch, could indicate different feeding processes. Indeed, Odonne et al. (2021) studied flat-topped and conical Mvs in Azerbaijan and suggest that the flat-topped are regularly fed and constantly deforming, while the conical have episodic but more violent eruptions.

The flat-topped Mvs are located where the seafloor is about 500 m deep and at the top of the eroded anticline of the Lee Arch and thus with shallow source rocks. The cone-shaped Mvs are located on the flank of the Lee Arch at about 700 m depth and with deep source rocks. Therefore, the fluid overpressure required for gas and mud migration could be lower for flat-topped Mvs, which can be fed continuously, and higher for the cone-shapes Mvs, where it would take some time to reach the required overpressure with a consequently violent explosion. The morphological evidence of scarp and debris flow of Mv19 in area B, also indicate in this area an episodic violent eruption.

Features associated with a violent explosion include the diatreme located on the flank of Lee Arch, (Fig. 6). Pockmarks, negative morphologies formed as a result of concentrated fluid flows (Hovland, 2008), are also present in the area A (Fig. 3) and were also documented by Lawver and Davis (2007, 2012). Downward deflected reflections forming apparent depressions beneath the mud volcanoes and pockmarks (Fig. 6) may be considered collapse features due to volume depletion, as suggested by Andresen et al. (2010).

5.4. The new perspective of a possible biological activity related to fluid seepages in extreme environments

Ocean research in recent decades has provided evidence of a variety of deep-sea ecosystems, which in some cases are associated to seepages of fluids, mud volcanoes and gas hydrate/free gas-bearing sea floor sediment.

In the marine environment, the fluid seeps often provide methane and sulfide fluxes that feed consortia of methanotrophic archea and sulfate-reducing bacteria that release bicarbonate and hydrogen sulfide into the pore water. This triggers additional biogeochemical processes providing precipitation of methane-derived authigenic carbonates and precipitation of solid iron sulphide, both of which provide a substrate on which other species can live (Freiwald and Roberts, 2006 and ref. therein).

Hence, deep-sea fluid seepage sites may be hotspots of biodiversity and provide a nursery, refuge or preferred substrate for a wide variety of associated cold-water communities (Roberts et al., 2006), as foraminifera, gastropods, brachiopods, bivalves, echinoids bryozoa, sponges and gorgonias, crustaceans, cnidarians, polychaetes, crinoids, hydroids and fish (e.g. Jensen and Frederiksen 1992; Mortensen et al., 1995; Rogers 1999; Dorschel et al., 2007; Freiwald et al., 2021).

In Antarctica, evidence of chemotrophic ecosystems were found beneath the former Larsen B Ice Shelf (Antarctic Peninsula) in a 850 m deep glacial through, constituted by an association of microbial mats with gas bubbles emission (presumably methane with hydrogen sulphide), cold seep clam communities, and small mounds (1.5–2 m across and 0.75 m high) with mudflows and large bivalves encircled around the central orifice (Domack et al., 2005). The findings clearly indicate that polar environments are not a limit to the occurrence of these unique communities. Similarly, also the mud volcanoes in the Ross Sea may host chemically based ecosystems. The extreme polar environment of the Ross Sea does not prevent the life of carbonate organisms, as corals, bryozoans, and other carbonate species have been recovered from the sea floor (Remia et al., 2003).

The occurrences of gryphons, between the Iulia and Tergeste MV, and on the mounds, could be the preferred sites for the development of chemio-synthetic ecosystems.

6. Conclusions

An in-depth analysis, following a targeted reprocessing of geophysical data in the Ross Sea area, has identified five provinces characterized by the presence of mud volca-

noes are located on the seafloor or buried under sediment. In one of these provinces, the OGS Explora Mounds, there are several dozen of mud conical/elongated and flat-topped mud volcanoes occurring at seafloor in an area of about 30 km × 40 km. They can vary in size, reaching more than 5 km in diameter and tens of metres in height.

The mud volcanoes may be due to a cold seep system consisting of Miocene (or older) source rocks, a plumbing system with pipes, chimneys, fault conduits, forced folds and seafloor seeps that have formed mud volcanoes, pockmarks and diatreme, or due to the combination of gravitational instability of clayey sediment and fluid overpressure.

The provinces are related to different geological settings, such as the transpressional structure of the Lee Arch where tectonics control the plumbing system, and in sedimentary basins, where the mud volcanism is probably caused mainly by gravitative instability of the sediment that rises by buoyancy.

This study provides evidence that these features are quite common in the Ross Sea, and may represent unique biodiversity hotspots for extreme environments such as the seafloor of the Antarctic continental shelf.

Mud volcanoes release large amounts of methane into the water column, and potentially into the atmosphere, and the identification of the active provinces can provide information for the endogenous contribution to the global greenhouse gas budget.

CRediT authorship contribution statement

Martina Busetti: Conceptualization, Data curation, Funding acquisition, Investigation, Methodology, Writing – original draft, Writing – review & editing. **Riccardo Geletti:** Conceptualization, Data curation, Funding acquisition, Investigation, Methodology, Writing – original draft, Writing – review & editing. **Dario Civile:** Data curation, Methodology, Writing – review & editing. **Chiara Sauli:** Data curation, Methodology, Writing – review & editing. **Giuseppe Brancatelli:** Data curation, Methodology, Writing – review & editing. **Edy Forlin:** Data curation, Methodology, Writing – review & editing. **Daniela Accettella:** Data curation, Methodology. **Lorenza Barro Savonuzzi:** Data curation, Methodology. **Laura De Santis:** Data curation, Writing – review & editing. **Aldo Vesnaver:** Data curation, Methodology, Writing – review & editing. **Andrea Cova:** Investigation, Methodology.

Declaration of Competing Interest

The authors declare that they have no known competing financial interests or personal relationships that could have appeared to influence the work reported in this paper.

Acknowledgements

The data used were collected during several cruises. The multichannel seismic profiles are available through the Antarctic Seismic Data Library System for Cooperative Research (https://sdls.ogs.trieste.it).

The swath bathymetry data (MB) and the chirp sub-bottom profilers in the western Ross Sea were acquired in 2006 among the PNRA project "Framing the kinematics and timing of the Cenozoic tectonics in the VIctoria LanD/Ross Sea region within the activity of the Southern Ocean Fracture Zones (VILD)", and we thank the Captain F. Sedmak, the crew and OGS engineers and technicians of the R/V OGS Explora for their assistance during the cruises, in particular driving the ship in extreme sea ice conditions. The PNRA OGS multichannel seismic data collected in 1988 and 1990 was revisited and reprocessed among the PNRA project "Seismic data VALorization: methods for FLUid detection within polar sediments and study for georisk and environment (VALFLU)".

The BGR and USGS seismic data were made available among collaborative projects and reprocessed by L. Barro Savonuzzi for the master thesis in the frame of the PNRA18_00002 ANTIPODE Project and published in Barro Savonuzzi et al., (2023).

The authors thank the IHS Markit® of S&P Global that provide the educational licence of the Kingdom™ software for seismic interpretation, the Aspen Technology Inc for the academic licences of Echos and Geodepth, Promax from Landmark, and the Schlumberger® for the educational and academic licences of Vista® software, for seismic processing, Teledyne Reson PDS2000 and Teledyne Caris software for multibeam data processing.

References

Andresen, K.J., 2012. Fluid flow features in hydrocarbon plumbing systems: What do they tell us about the basin evolution? Mar. Geol. 332–334, 89–108. https://doi.org/10.1016/j.margeo.2012.07.006.

Andresen, K.J., Clausen, O.R., Jørgesen, R.B., 2010. A composite mud volcano system in the Chalk Group of the North Sea Central Graben. J. Geol. Soc. London 167, 1209–1224. https://doi.org/10.1144/0016-76492010-037.

Barrett, P. J. and Scientific Staff, 1985. Plio-Pleistocene glacial sequence cored at CIROS 2 Ferrar Fjord, western McMurdo Sound. Victoria University Antarctic Research Expedition Science and Logistics Reports VUWAE 29, 6, 2, 8-19.

Barrett, P. J., 1986. Antarctic Cenozoic history from the MSSTS-1 drillhole, McMurdo Sound, Antarctica. New Zealand Department of Scientific and Industrial Research Bulletin 237, 174 pp.

Barrett, P. J., 1989. Antarctic Cenozoic history from the CIROS-1 drillhole, McMurdo Sound, Antarctica. New Zealand Department of Scientific and Industrial Research Bulletin, 245, 254 pp.

Barro Savonuzzi, L., Brancatelli, G., Forlin, E., De Santis, L., Geletti, R., Busetti, M., Wardell, N., Del Ben, A., 2023. Miocene mounds on the Ross Sea paleo-continental shelf: evidence of the onset of Antarctic glaciations or mud volcanoes? Bulletin of Geophysics and Oceanography 64 (3), 1–20. https://doi.org/10.4430/bgo00417.

Bart, P.J., Anderson, J.A., Trincardi, F., Shipp, S.S., 2000. Seismic data from the Northern Basin, Ross Sea, record extreme expansions of the East Antarctic Ice Sheet during the late Neogene. Mar. Geol. 166 (1–4), 31–50. https://doi.org/10.1016/S0025-3227(00)00006-2.

Bart, P.J., Sjunneskog, C., Chow, J.M., 2011. Piston-core based biostratigraphic constraints on Pleistocene oscillations of the West Antarctic Ice Sheet in western Ross Sea between North Basin and AND-1B drill site. Mar. Geol. 289 (1–4), 86–99. https://doi.org/10.1016/j.margeo.2011.09.005.

Behrendt, J.C., LeMasurier, W.E., Cooper, A.K., Tessensohn, F., Tréhu, A., Damaske, D., 1991. Geophysical studies of the West Antarctic Rift System. Tectonics 10 (6), 1257–1273. https://doi.org/10.1029/91TC00868.

Boehm, G., Brancolini, G., Fais, S., Snidarcig, A., Vesnaver, A., 1993. Integrated interpretation of geophysical anomalies in the western Ross Sea (Antarctica). Boll. Geofis. Teor. Appl. 35 (137–138), 119–132.

Brancatelli, G., Forlin, E., Bertone, N., Del Ben, A., Geletti, R., 2022. Time to depth seismic reprocessing of vintage data: A case study in the Otranto Channel (South Adriatic Sea). In: Rebecca Bell, David Iacopini, Mark Vardy, (Eds) Interpreting Subsurface Seismic Data. Elsevier, pp. 157-197. 10.1016/B978-0-12-818562-9.00009-1.

Brancolini, G., Busetti, M., Coren, F., De Cillia, C., Marchetti, M., De Santis, L., Zanolla, C., Cooper, A.K., Cochrane, G.R., Zayatz, I., Belyaev, V., Knyazev, M., Vinnikovskaya, O., Davey, F.J., Hinz, K., 1995. ANTOSTRAT Project, seismic stratigraphic atlas of the Ross Sea, Antarctica. In: Cooper, A.K., Barker, P.F., Brancolini, G., (Eds.), Geology and Seismic Stratigraphy of the Antarctic Margin. Antarctic Research Series, vol. 68, AGU Washington, D.C. 20 tables.

Cape Roberts Science Team, 1998. Initial report on CRP-1, Cape Roberts Project. Terra Antartica 5(5), 1-187.

Cape Roberts Science Team, 1999. Studies from the Cape Roberts Project, Ross Sea, Antarctica, initial report on CRP-2/2A. Terra Antartica 6, 1-173.

Cape Roberts Science Team, 2000. Studies from the Cape Roberts Project, Ross Sea, Antarctica, initial report on CRP-3/3A. Terra Antartica 7, 1-209.

Cartwright, J., Santamarina, C., 2015. Seismic characteristics of fluid escape pipes in sedimentary basins: Implications for pipe genesis. Mar. Pet. Geol. 65, 126–140. https://doi.org/10.1016/j.marpetgeo.2015.03.023.

Chow, J.M., Bart, P.J., 2003. West Antarctic Ice Sheet grounding events on the Ross Sea outer continental shelf during the middle Miocene. Palaeogeogr. Palaeoclimatol. Palaeoecol. 198 (1–2), 169–186. https://doi.org/10.1016/S0031-0182(03)00400-0.

Claerbout, J., 1985. Imaging the Earth's Interior. Blackwell, Oxford, UK, p. 398.

Claypool, G., Kvenvolden, K., 1983. Methane and other hydrocarbon gases in marine sediment. Annu. Rev. Earth Planet. Sci. 11, 299–327. https://doi.org/10.1146/annurev.ea.11.050183.001503.

Collen J. D., Xinghua Y., Collier R. J., Johnston, J. H., 1989. Hydrocarbon source rock potential and organic maturation. In: Barrett, P. (Ed.), Antarctic Cenozoic history

from the CIROS-1 drillhole, McMurdo Sound. DSIR Bulletin, Wellington, 245, 223-230.
Cook, R.W., Woolhouse, A.D., 1989. Hydrocarbon residue. In: Barrett, P., (Ed.), Antarctic Cenozoic history from the CIROS-1 drillhole, McMurdo Sound. DSIR Bulletin, Wellington, 245, 211-217.
Cooper, A.K., Davey, F.J., Behrendt, J.C., 1987. Seismic stratigraphy and structure of the Victoria Land Basin, Western Ross Sea, Antarctica. In: Cooper, A.K., Davey, F. J. (Eds.), The Antarctic Continental Margin: Geology and Geophysics of the Western Ross Sea. Circum-Pacific Council of Energy and Mineral Resource Earth Science Series, Huston, Texas, vol. 5B, pp. 27–76.
Davey, F.J., Brancolini, G., Hamilton, R.J., Henrys, S., Sorlien, C.C., 2000. A revised correlation of the seismic stratigraphy at the Cape Roberts drill sites with the seismic stratigraphy of the Victoria Land Basin, Antarctica. Terra Antartica 7 (3), 215–220.
Denich, E., Vesnaver, A., Baradello, L., 2021. Amplitude recovery and deconvolution of Chirp and Boomer data for marine geology and offshore engineering. Energies 14, 1–14. https://doi.org/10.3390/en14185704.
Domack, E., Ishman, S., Leventer, A., Sylva, S., Willmott, V., Huber, B., 2005. Chemotrophic Ecosystem Beneath the Larsen Ice Shelf. EOS Trans. Am. Geophys. Union 86, 269–276. https://doi.org/10.1029/2005EO290001.
Dorschel, B., Hebbeln, D., Rüggeberg, A., Dullo, W.C., 2007. Carbonate budget of a cold-water coral carbonate mound: Propeller Mound, Porcupine Seabight. Int. J. Earth Sci. 96, 73–83. https://doi.org/10.1007/s00531-005-0493-0.
Dorschel, B., Hehemann, L., Viquerat, S., Warnke, F., Dreutter, S., Schulze, T.Y., Accettella, D., An, L., Barrios, F., Bazhenova, E., Black, J., Bohovo, F., Davey, C., De Santis, L., Escutia, D.C., Fremand, A.C., Fretwell, P.T., Gales, J.A., Gao, J., Gasperini, L., Greenbaum, J.S., Henderson, J.J., Hong, J.K., Jakobsson, M., Jensen, L., Kool, J., Larin, S., Larter, R.D., Leitchenkov, G., Loubrieu, B., Mackay, K., Mayer, L., Millan, R., Morlighem, M., Navidad, F., Nitsche, F.O., Nogi, Y., Pertuisot, C., Post, A.L., Pritchard, H.D., Purser, A., Rebesco, M., Rignot, E., Roberts, J.L., Rovere, M., Ryzhov, I., Sauli, C., Schmitt, T., Silvano, A., Smith, J., Snaith, H., Tate, A.J., Tinto, K., Vandenbossche, P., Weatherall, P., Wintersteller, P., Yang, C., Zhang, T., Arndt, J.E., 2022. The International Bathymetric Chart of the Southern Ocean Version 2. Sci. Data 9 (275), 1–13. https://doi.org/10.1038/s41597-022-01366-7.
Ferraccioli, F., Armadillo, E., Zunino, A., Bozzo, E., Rocchi, S., Armienti, P., 2009. Magmatic and tectonic patterns over the Northern Victoria Land sector of the Transantarctic Mountains from new aeromagnetic imaging. Tectonophysics 478, 43–61. https://doi.org/10.1016/j.tecto.2008.11.028.
Fielding, R.C., 2018. Stratigraphic architecture of the Cenozoic succession in the McMurdo Sound region, Antarctica: An archive of polar palaeoenvironmental change in a failed rift setting. Sedimentology 65, 1–61. https://doi.org/10.1111/sed.12413.
Fielding, C.R., Whittaker, J., Henrys, S.A., Wilson, T.J., Naish, T.R., 2008. Seismic facies and stratigraphy of the Cenozoic succession in McMurdo Sound, Antarctica: Implications for tectonic, climatic and glacial history. Palaeogeogr. Palaeoclimatol. Palaeoecol. 260, 8–29. https://doi.org/10.3133/of2007-1047.srp090.
Freiwald A., Rogers A., Hall-Spencer J., Guinotte J.M., Davies A.J., Yesson C., Martin C. S., Weatherdon L.V., 2021. Global distribution of cold-water corals (version 5.1). Fifth update to the dataset in Freiwald et al. (2004) by UNEP-WCMC, in collaboration with Andre Freiwald and John Guinotte. Cambridge (UK): UN Environment Programme World Conservation Monitoring Centre. Data: 10.34892/72x9-rt61.
Freiwald, A., Roberts, J.M., 2006. Cold-Water Corals and Ecosystems. SpringerBerlin, Heidelberg. 10.1007/3-540-27673-4.
Gantar, C., Zanolla, C., 1993. Gravity and magnetic exploration in the Ross Sea (Antarctica). Bollettino Di Geofisica Teorica e Applicata 35 (137–138), 219–230.
Gazdag, J., 1978. Wave equation migration with the phase-shift method. Geophysics 43, 1337–1556. https://doi.org/10.1190/1.1440899.
Geletti, R., Busetti, M., 2011. A double bottom simulating reflector in the western Ross Sea, Antarctica. J. Geophys. Res. Solid Earth 116 (B04101). https://doi.org/10.1029/2010JB007864.
Geletti, R., Busetti, M., 2022. Bottom Simulating Reflector in the Western Ross Sea, Antarctica. In: Mienert, J., Berndt, C., Tréhu, A.M., Camerlenghi, A., Liu, C.S. (Eds.), World Atlas of Submarine Gas Hydrates in Continental Margins. Springer, Cham, pp. 475–482. https://doi.org/10.1007/978-3-030-81186-0_40.
Geletti, R., Pipan, M., Vesnaver, A., 1993. Signal/Noise ratio enhancement of a seismic profile in the Ross Sea (Antarctica). Boll. Geofis. Teor. Appl. 35 (137–138), 173–193.
Giustiniani, M., Tinivella, U., Sauli, C., Della, V.B., 2018. Distribution of the gas hydrate stability zone in the Ross Sea. Antarctica. Andean Geology 45 (1), 78–86. https://doi.org/10.5027/andgeoV45n1-2989.
Greenwood, S.L., Simkins, L.M., Halberstadt, A.R.W., Protho, L.O., Anderson, J.B., 2018. Holocene reconfiguration and readvance of the East Antarctic Ice Sheet. Nature Communication 9, 3176. https://doi.org/10.1038/s41467-018-05625-3.
Hamilton, R., Sorlien, C.C., Luyendyk, B.P., Bartek, L.R., 2001. Cenozoic tectonics of the Cape Roberts rift basin and Transantarctic Mountains front, southwestern Ross Sea, Antarctica. Tectonics 20, 325–342. https://doi.org/10.1029/2000TC001218.
Hayes, D.E., Frakes, L.A., et al., 1975. Initial Reports of the Deep Sea Drilling Project., 28. U.S. Government Printing Office, Washington, DC. 1017 pp.
Horgan, H., Naish, T., Bannister, S., Balfour, N., Wilson, G., 2005. Seismic stratigraphy of the Plio-Pleistocene Ross Island flexural moatfill: A prognosis for ANDRILL Program drilling beneath McMurdo-Ross Ice Shelf. Global Planet. Change 45 (1–3), 83–97. https://doi.org/10.1016/j.gloplacha.2004.09.014.
Hovland, M., 2008. Do carbonate reefs form due to fluid seepage? Terra Nova 2, 8–18. https://doi.org/10.1111/j.1365-3121.1990.tb00031.x.
Jensen, A., Frederiksen, R., 1992. The fauna associated with the banck-forming deepwater coral Lophelia pertusa (Scleractiniaria) on the Faroe shelf. Sarsia 77, 53–69. https://doi.org/10.1080/00364827.1992.10413492.
Kopf, A.J., 2002. Significance of mud volcanism. Rev. Geophys. 40, 1–52. https://doi.org/10.1029/2000RG000093.
Kulhanek, D.K., Levy, R.H., Clowes, C.D., Prebble, J.G., Rodelli, D., Jovane, L., Morgans, H.E.G., Kraus, C., Zwingmann, H., Griffith, E.M., Scher, H.D., McKay, R.M., Naish, T.R., 2019. Revised chronostratigraphy of DSDP Site 270 and late Oligocene to early Miocene paleoecology of the Ross Sea sector of Antarctica. Global Planet. Change 178, 46–64. https://doi.org/10.1016/j.gloplacha.2019.04.002.
Kyle, P.R., Moore, J.A., Thirlwall, M.F., 1992. Petrologic evolution of anorthoclase phonolite lavas at Mount Erebus, Ross Island, Antarctica. J. Pet. 33, 849–875. https://doi.org/10.1093/petrology/33.4.849.
Lawver, L. A., Davis, M. B., Wilson, T. J. and shipboard scientific party, 2007. Neotectonic and other features of the Victoria Land Basin, Antarctica, interpreted from multibeam bathymetry data. In: Cooper A.K., Raymond C.R., et al., (Eds.), Antarctica: A Keystone in a Changing World. Online Proceedings of the 10th ISAES X, USGS Open-File Report 2007-1047, Extended Abstract 017, 4 p.
Lawver, L., Lee, J., Kim, Y., Davey, F., 2012. Flat-topped mounds in western Ross Sea: carbonate mounds or subglacial volcanic features? Geosphere 8 (3), 645–653. https://doi.org/10.1130/GES00766.1.
LeMasurier, W.E., Thomson, J.W., Baker, P.E., Kyle, P.R., Rowley, P.D., Smellie, J.L., Verwoerd, W.J., 1990. Volcanoes of the Antarctic Plate and Southern Ocean. Antarctic Research Series, 48, American Geophysical Union, Washington, D.C., 487 pp. 10.1029/AR048.
Løseth, H., Gading, M., Wensaas, L., 2009. Hydrocarbon leakage interpreted on seismic data. Mar. Pet. Geol. 26, 1304–1319. https://doi.org/10.1016/j.marpetgeo.2008.09.008.
Mazzini, A., Etiope, G., 2017. Mud volcanism: an updated review. Earth-Science Review 168, 81–112. https://doi.org/10.1016/j.earscirev.2017.03.001.
McIver, R. D., 1975. Hydrocarbon gases in canned core samples from Leg 28 sites 271, 272, and 273, Ross Sea. In: Hayes, D. E., Frakes, L. A., et al., (Eds.), Initials reports of the Deep Sea Drilling Project, v. 28, Washington, DC (US Government Printing Office), pp. 815-817. http://dx.doi.org/10.2973/dsdp.proc.28.128.1975.
McKay, R.M., De Santis, L., Kulhanek, and the Expedition 374 Scientists, 2019. Ross Sea West Antarctic Ice Sheet History. Proceedings of the International Ocean Discovery Program, 374: College Station, TX (International Ocean Discovery Program). 10.14379/iodp.proc.374.2019.
Mortensen, P.B., Hovland, M., Brattegard, T., Farestveit, R., 1995. Deep water bioherms of the scleractinian coral Lophelia pertusa (L.) at 64°N on the Norwegian Shelf: structure and associated megafauna. Sarsia 80 (2), 145–158. https://doi.org/10.1080/00364827.1995.10413586.
Naish, T., Powell, R., Levy, R., 2007. Studies from the ANDRILL McMurdo Ice Shelf Project, Antarctica: Initial science report on AND-1B. Terra Antartica 14 (3), 328.
Naish, T., Powell, R., Levy, R., Wilson, G., Scherer, R., Talarico, F., Krissek, L., Niessen, F., Pompilio, M., Wilson, T., Carter, L., DeConto, R., Huybers, P., McKay, R., Pollard, D., Ross, J., Winter, D., Barrett, P., Browne, G., Cody, R., Cowan, E., Crampton, J., Dunbar, G., Dunbar, N., Florindo, F., Gebhardt, C., Graham, I., Hannah, M., Hansaraj, D., Harwood, D., Helling, D., Henrys, S., Hinnov, L., Kuhn, G., Kyle, P., Läufer, A., Maffioli, P., Magens, D., Mandernack, K., McIntosh, W., Millan, C., Morin, R., Ohneiser, C., Paulsen, T., Persico, D., Raine, I., Reed, J., Riesselman, C., Sagnotti, L., Schmitt, D., Sjunneskog, C., Strong, P., Taviani, M., Vogel, S., Wilch, T., Williams, T., 2009. Obliquity-paced Pliocene West Antarctic Ice Sheet oscillations. Nature 458, 322–328. https://doi.org/10.1038/nature07867.
Odonne, F., Imbert, P., Remy, D., Gabalda, G., Aliyev, A.A., Abbasov, O.R., Baloglanov, E.E., Bichaud, V., Juste, R., Dupuis, M., Bonvalot, S., 2021. Surface structure, activity and microgravimetry modeling delineate contrasted mud chamber types below flat and conical mud volcanoes from Azerbaijan. Mar. Pet. Geol. 134, 1–24. https://doi.org/10.1016/j.marpetgeo.2021.105315.
Pekar, S.F., Speece, M.A., Wilson, G.S., Sunwall, D.S., Tinto, K.J., 2013. The Offshore New Harbour Project: Deciphering the Middle Miocene through Late Eocene seismic stratigraphy of Offshore New Harbour, western Ross Sea, Antarctica. Geological Society of London Special Publications 381 (1), 199–213. https://doi.org/10.1144/SP381.2.
Pérez L.F., De Santis L., McKay R.M., Larter R.D., Ash J., Bart P.J., Böhm G., Brancatelli G., Browne I., Colleoni F., Dodd J.P., Geletti R., Harwood D.M., Kuhn G., Sverre Laberg J., Leckie R.M., Levy R.H., Marschalek J., Mateo Z., Naish T.R., Sangiorgi F., Shevenell A.E., Sorlien C.C., Flierdt T. van de, IODP Expedition 374 Scientists, 2021. Early and middle Miocene ice sheet dynamics in the Ross Sea: results from integrated core-log-seismic interpretation. GSA Bull., 134, 3487-370. https://doi.org/10.1130/B35814.1.
Pérez, L.F., McKay, R.M., Santis, L.D., Larter, R.D., Levy, R.H., Naish, T.R., Anderson, J. A., Bart, P.J., Busetti, M., Dunbar, G., Sauli, C., Sorlien, C.C., Speece, M., 2022. Miocene ice sheet dynamics in the westernmost Ross Sea (Antarctica): Regional correlations. Global Planet. Change 216, 10391. https://doi.org/10.1016/j.gloplacha.2022.103891.
Prothro, L.O., Majewski, W., Yokoyama, Y., Simkins, L.M., Anderson, J.B., Yamane, M., Miyairi, Y., Ohkouchi, N., 2020. Timing and pathways of East Antarctic Ice Sheet retreat. Quat. Sci. Rev. 230, 106166. https://doi.org/10.1016/j.quascirev.2020.106166.

Rapp, J. B., Kvenvolden, K. A., Golan-Bac, M., 1987. Hydrocarbon geochemistry of sediments offshore from Antarctica. In: Cooper, A. K., Davey, F. J., (Eds.), The Antarctic Continental Margin: Geology and Geophysics of the Western Ross Sea. Circum-Pacific Council of Energy and Mineral Resource Earth Science Series, vol. 5B, Huston, Texas, pp. 217-224.

Remia, A., Hart, C., Oliverio, M. Taviani M., 2003. Bottom carbonate production in Little America Basin, Ross Sea, Antarctica. In: Proceedings of the 4th Meeting on Italian Antarctic Glaciology (4th CONGA), Milan, 25-26 June 2002. Terra Antarctica Reports, 8, 153-157.

Revil, A., 2002. Genesis of mud volcanoes in sedimentary basins: a solitary wave-based mechanism. Geophysical Research Letters 29(12), 15-1-15-4. https://doi.org/10.1029/2001GL014465.

Rilling, S., Mukasa, S., Wilson, T., Lawver, L., Hall, C., 2009. New determinations of 40Ar/39Ar isotopic ages and flow volumes for Cenozoic volcanism in the Terror Rift, Ross Sea, Antarctica. J. Geophys. Res. 114/, B12207. https://doi.org/10.1029/2009JB006303.

Roberts, J.M., Wheeler, A.J., Freiwald, A., 2006. Reefs of the deep: the biology and geology of cold-water coral ecosystems. Science 312 (5773), 543–547. https://doi.org/10.1126/science.1119861.

Rogers, A.D., 1999. The biology of Lophelia pertusa (Linnaeus 1758) and other deep-water reef-forming corals and impacts from human activities. International Review Hydrobiology 84 (4), 315–406.

Salvini, F., Brancolini G., Busetti M., Storti F., Mazzarini F., Coren F., 1997. Cenozoic geodynamics of the Ross Sea region, Antarctica: Crustal extension, intraplate strike-slip faulting, and tectonic inheritance, Journal of Geophysical Research 102(B11), 24,669- 24,696. https://doi.org/10.1029/97JB01643.

Sauli, C., Busetti, M., De Santis, L., Wardell, N., 2014. Late Neogene geomorphological and glacial reconstruction of the northern Victoria Land coast, western Ross Sea (Antarctica). Mar. Geol. 355 (1), 297–309. https://doi.org/10.1016/j.margeo.2014.06.008.

Sauli, C., Sorlien, C., Busetti, M., De Santis, L., Geletti, R., Wardell, N., Luyendyk, B.P., 2021. Neogene development of the Terror Rift, western Ross Sea, Antarctica. Geochemistry, Geophysics, Geosystems 22,. https://doi.org/10.1029/2020GC009076 e2020GC009076.

Savage, M.L., Ciesielsky, P.F., 1983. Revised History of Glacial Sedimentation in the Ross Sea Region. In: Proceedings of the Fourth International Symposium on Antarctic Earth Sciences. University of Adelaide, South Australia, pp. 555–559.

Ship, S., Anderson, J., Domack, E., 1999. Late Pleistocene-Holocene retreat of the West Antarctic Ice-Sheet system in the Ross Sea: part 1 - geophysical results. Geol. Soc. Am. Bull. 111 (10), 1486–1516.

Sloan, E.D., 1990. Clathrate Hydrates of Natural Gases. Marcel Dekker, New York, p. 641.

Smellie, J.L., Rocchi, S., Armienti, P., 2011. Late Miocene volcanic sequences in northern Victoria Land, Antarctica: products of glaciovolcanic eruptions under different thermal regimes. Bull. Volcanol. 73 (1), 1–25. https://doi.org/10.1007/s00445-010-0399-y.

SMS Science Team, 2010. An integrated age model for the ANDRILL-2A drill core. In: K. Kontar, D.M. Harwood, F. Florindo, S. Fischbein (Compilers), ANDRILL Southern McMurdo Sound Project Science Integration Workshop, Erice, Italy, 6–11th April, 2010, ANDRILL Contribution 16, 12-13.

Sorlien, C., Luyendyk, B., Bartek L., 2010. Multi-Channel Seismic Shot Data from McMurdo Sound, Antarctica acquired during the R/V Nathaniel B. Palmer expedition NBP0301 (2003). Interdisciplinary Earth Data Alliance (IEDA). doi:10.1594/IEDA/315814.

Sorlien, C.C., Luyendyk, B.P., Decesari, R.C., Wilson, D.S., Bartek, L.R., 2007. Oligocene development of the West Antarctic Ice Sheet recorded in eastern Ross Sea strata. Geolog. Soc. Am. 35 (5), 467–470. https://doi.org/10.1130/G23387A.1.

Taner, M.T., Koehler, F., Sheriff, R.E., 1979. Complex seismic trace analysis. Geophysics 44, 1041–1063. https://doi.org/10.1190/1.1440994.

ten Brink, U.S., Schneider, C., Johnson, A.H., 1995. Morphology and stratal geometry of the Antarctic continental shelf: Insights from models. In: Cooper, A.K., Barker, P.F., Brancolini, G. (Eds.), Geology and seismic stratigraphy of the Antarctic margin, In: Antarctic Research Series AGU, 68. AGU, Washington, D.C, pp. 1–24. https://doi.org/10.1029/AR068p0001.

Wangen, M., 2022. Models of overpressure build-up in shallow sediments by glacial deposition and glacial loading with respect to chimney formation. Modeling Earth Syst. Environ. 8, 1227–1242. https://doi.org/10.1007/s40808-020-01064-6.

Weigelt, E., Uenzelmann-Neben, G., Gohl, K., Larter, R.D., 2012. Did massive glacial dewatering modify sedimentary structures on the Amundsen Sea Embayment shelf, West Antarctica?. Global Planet. Change 92–93, 8–16. https://doi.org/10.1016/j.gloplacha.2012.04.006.